



**UNIVERSIDAD DE INVESTIGACIÓN DE  
TECNOLOGÍA EXPERIMENTAL YACHAY**

**Escuela de Ciencias Químicas e Ingeniería**

**TÍTULO: Chitosan-based hydrogel for wastewater treatment**

Trabajo de integración curricular presentado como requisito  
para la obtención del título de Química

**Autora:**

López Aveiga Melany Gisell

**Tutora:**

Ph.D. Michell Uribe Rose Mary

**Co-tutora:**

Ph.D. Floralba López

Urcuquí, septiembre 2020



Urucuquí, 16 de septiembre de 2020

**SECRETARÍA GENERAL**  
**(Vicerrectorado Académico/Cancillería)**  
**ESCUELA DE CIENCIAS QUÍMICAS E INGENIERÍA**  
**CARRERA DE QUÍMICA**  
**ACTA DE DEFENSA No. UITEY-CHE-2020-00045-AD**

A los 16 días del mes de septiembre de 2020, a las 15:00 horas, de manera virtual mediante videoconferencia, y ante el Tribunal Calificador, integrado por los docentes:

<b>Presidente Tribunal de Defensa</b>	Dr. CAETANO SOUSA MANUEL , Ph.D.
<b>Miembro No Tutor</b>	Dr. TAFUR GUISAO, JUAN PABLO , Ph.D.
<b>Tutor</b>	Dra. MICHELL URIBE, ROSE MARY RITA , Ph.D.

El(la) señor(ita) estudiante **LOPEZ AVEIGA, MELANY GISELL**, con cédula de identidad No. **1004058044**, de la **ESCUELA DE CIENCIAS QUÍMICAS E INGENIERÍA**, de la Carrera de **QUÍMICA**, aprobada por el Consejo de Educación Superior (CES), mediante Resolución **RPC-SO-39-No.456-2014**, realiza a través de videoconferencia, la sustentación de su trabajo de titulación denominado: **CHITOSAN BASED HYDROGEL FOR WASTEWATER TREATMENT** , previa a la obtención del título de **QUÍMICO/A**.

El citado trabajo de titulación, fue debidamente aprobado por el(los) docente(s):

<b>Tutor</b>	Dra. MICHELL URIBE, ROSE MARY RITA , Ph.D.
--------------	--

Y recibió las observaciones de los otros miembros del Tribunal Calificador, las mismas que han sido incorporadas por el(la) estudiante.

Previamente cumplidos los requisitos legales y reglamentarios, el trabajo de titulación fue sustentado por el(la) estudiante y examinado por los miembros del Tribunal Calificador. Escuchada la sustentación del trabajo de titulación a través de videoconferencia, que integró la exposición de el(la) estudiante sobre el contenido de la misma y las preguntas formuladas por los miembros del Tribunal, se califica la sustentación del trabajo de titulación con las siguientes calificaciones:

Tipo	Docente	Calificación
Tutor	Dra. MICHELL URIBE, ROSE MARY RITA , Ph.D.	10,0
Miembro Tribunal De Defensa	Dr. TAFUR GUISAO, JUAN PABLO , Ph.D.	10,0
Presidente Tribunal De Defensa	Dr. CAETANO SOUSA MANUEL , Ph.D.	9,7

Lo que da un promedio de: **9.9 (Nueve punto Nueve)**, sobre 10 (diez), equivalente a: **APROBADO**

Para constancia de lo actuado, firman los miembros del Tribunal Calificador, el/la estudiante y el/la secretario ad-hoc.

Certifico que *en cumplimiento del Decreto Ejecutivo 1017 de 16 de marzo de 2020, la defensa de trabajo de titulación (o examen de grado modalidad teórico práctica) se realizó vía virtual, por lo que las firmas de los miembros del Tribunal de Defensa de Grado, constan en forma digital.*

**LOPEZ AVEIGA, MELANY GISELL**  
**Estudiante**

**Dr. CAETANO SOUSA MANUEL , Ph.D.**  
**Presidente Tribunal de Defensa**

MANUEL  
 CAETANO SOUSA  
 Digitally signed by  
 MANUEL CAETANO SOUSA  
 Date: 2020.09.16 15:43:11  
 -05'00'

**Dra. MICHELL URIBE, ROSE MARY RITA , Ph.D.**  
**Tutor**

ROSE MARY  
 RITA MICHELL  
 URIBE  
 Firmado digitalmente  
 por ROSE MARY RITA  
 MICHELL URIBE  
 Fecha: 2020.09.16  
 15:33:52 -05'00'





## AUTORÍA

Yo, **Melany Gisell López Aveiga**, con cédula de identidad 1004058044, declaro que las ideas, juicios, valoraciones, interpretaciones, consultas bibliográficas, definiciones y conceptualizaciones expuestas en el presente trabajo; así como, los procedimientos y herramientas utilizadas en la investigación, son de absoluta responsabilidad de el/la autora (a) del trabajo de integración curricular. Así mismo, me acojo a los reglamentos internos de la Universidad de Investigación de Tecnología Experimental Yachay.

Urcuquí, septiembre 2020.



---

Melany Gisell López Aveiga

CI: 1004058044





## AUTORIZACIÓN DE PUBLICACIÓN

Yo, **Melany Gisell López Aveiga**, con cédula de identidad 1004058044, cedo a la Universidad de Investigación de Tecnología Experimental Yachay, los derechos de publicación de la presente obra, sin que deba haber un reconocimiento económico por este concepto. Declaro además que el texto del presente trabajo de titulación no podrá ser cedido a ninguna empresa editorial para su publicación u otros fines, sin contar previamente con la autorización escrita de la Universidad.

Asimismo, autorizo a la Universidad que realice la digitalización y publicación de este trabajo de integración curricular en el repositorio virtual, de conformidad a lo dispuesto en el Art. 144 de la Ley Orgánica de Educación Superior

Urququí, septiembre 2020.



---

Melany Gisell López Aveiga

CI: 1004058044



## **Dedication**

Dedicated to my parents, Edison and Angelita.

Melany Gisell López Aveiga



## **Acknowledgments**

First, I would like to express my gratitude to my parents Edison and Angelita, for their love, support, prayers, and sacrifices that made daily for me, to encouraged me to overcome difficulties and achieve my goals. My special thanks and gratitude to my advisor Ph.D. Rose Mary Michell, a great researcher at YachayTech University, for allowing me to do research and providing invaluable guidance throughout this work. As well as my co-advisor Ph.D. Floralba López for her support and guidance in this work. Besides, I would like to thank my professors of Yachay Tech for the knowledge they shared with me throughout my career has allowed me to get to where I am today. Also, I thank Ph.D. Alejandro Müller for allowing me to be part of his group during my stay in Polymat and provide me with the facilities so that my thesis can be carried out. To Connie Ocando, for her guidance and hospitality during my stay. I also thank all the staff of Yachay Tech University who, during my instance in the campus has supported me in several ways to complete this thesis successfully. I would like to say thanks to all my friends and research colleagues for the cooperation that extended me during these years. To all my family for all the support that gave me during this process. Finally, my thanks go to all the people who have supported me to complete my undergraduate thesis directly or indirectly.

Melany Gisell López Aveiga



## **RESUMEN:**

Los hidrogeles a base de quitosano se desarrollaron en este trabajo mediante dos métodos: goteo y evaporación del disolvente. La incorporación de nanopartículas magnéticas a los hidrogeles se realizó mediante coprecipitación in situ, y se utilizó glutaraldehído como reticulante en diferentes concentraciones (0.35% y 0.75%). Las muestras se caracterizaron por SEM, TGA y XDR. El análisis morfológico revela un cambio de porosidad de las muestras al agregar diferentes concentraciones de reticulante y nanopartículas. El aumento de la cantidad de reticulante implica una disminución del tamaño poroso; al mismo tiempo, la adición de nanopartículas de magnetita sugiere un cambio significativo en el diámetro del tamaño de los poros. Las propiedades térmicas se ven afectadas por las condiciones de reticulación al reducir su estabilidad con la adición de reticulante. Además, el trabajo proporciona información sobre un desarrollo reciente en la preparación, morfología y aplicación de hidrogeles nanocompuestos a base de quitosano utilizados para la eliminación de contaminantes acuosos.

**Palabras clave:** Hidrogeles basados en CS, Nanocompositos, Tratamiento de aguas residuales, Nanopartículas de magnetita





## **ABSTRACT:**

Chitosan-based hydrogels were developed in this work by two methods: drip and solvent evaporated. The incorporation of magnetic nanoparticles into the hydrogels was performed by in situ co-precipitation, and glutaraldehyde was used as a crosslinker in different concentrations (0.35% and 0.75%). Samples were characterized by SEM, TGA, and XDR. The morphology analysis reveals a porosity change of the samples by adding different concentrations of crosslinker and nanoparticles. The increase in the amount of crosslinker involves a decrease in porous size; concurrently, the addition of magnetite nanoparticles suggest a significant change in the pore size diameter. The thermal properties are affected by the crosslinking conditions by reducing its stability with the addition of crosslinker. Moreover, the work provides information about a recent development in the preparation, morphology, and application of chitosan-based nanocomposites hydrogels used for the removal of aqueous pollutants.

**Keywords:** CS-based hydrogels, Nanocomposites, Wastewater treatment. Magnetite nanoparticles



## INDEX

1. Introduction .....	1
2. Background .....	4
2.1 Preparation of chitosan-based hydrogels.....	4
2.1.2 Freeze drying technique .....	4
2.1.3 Cryogelation .....	6
2.1.4 Gas foaming .....	6
2.2 Properties of hydrogels.....	10
2.2.1 Swelling.....	10
2.2.2 Thermal Stability.....	11
2.2.3 Mechanical properties .....	13
2.3 Application of CS-based Nanocomposite Hydrogels for pollutant removal .....	15
2.3.1 Dye removal .....	15
2.3.2 Potentially toxic metals .....	18
3. Objectives.....	22
3.1 General Objective.....	22
3.2 Specific Objectives.....	22
4. Methodology .....	23
4.1 Materials.....	23
4.2 Experimental Description.....	23
4.2.1 Chitosan solution.....	23
4.2.2 Iron chitosan solution .....	23
4.2.3 Drip Method .....	23
4.2.4 Solvent Evaporated Method .....	24
4.3 Scanning Electron Microscope (SEM).....	26
4.4 Thermogravimetric Analysis (TGA).....	26
4.5 X-Ray Diffraction (XRD). .....	26
5. Results and Discussion.....	27
5.1 Morphology of CS-Based Hydrogel Nanocomposites .....	27
5.2 X-Ray diffraction (XRD) .....	29
5.3 Swelling.....	31
5.4 Thermal stability .....	32
6. Conclusion.....	39
7. Annex 1 .....	40
8. REFERENCES.....	45



## 1. Introduction

The proliferation of the industries impacts the planet by the pollution that it involves; one of the main affected aspects is water since industries such as textiles, tanneries, washing machines, among others, emit effluents in which potentially toxic metals are found. These metals of particular concern include zinc, copper, nickel, mercury, cadmium, lead, and chromium. [1] The main problem with these metals is that they are not biodegradable and tend to accumulate in living organisms, and many of these are known to be toxic or carcinogenic. [2] Therefore, an eco-friendly method is needed to be developed to remove the pollutants from water.

For the treatment of contaminated water, different methods have been used, including chemical precipitation, ion exchange, biological treatment, membrane separation, adsorption, and others. [3] Among these methods, adsorption is the focus of greatest scientific interest because it is easy to handle, present high efficiency, and it's an economical method for water treatment. In this context, hydrogels properties enable to be applied as adsorbents for various metal ions present in aqueous solution. [4]

Hydrogels are polymeric materials, which consist of three-dimensionally crosslinked networks, in which polymer chain presents hydrophilic groups such as hydroxyl, carboxyl, or amide, which allow the polymer to hold a large amount of water without dissolve in it. [5] Moreover, their abilities to respond to a variety of changes in the surrounding medium make them suitable for wide applications as drug delivery, and water treatment. [6] Polysaccharides, considered the most abundant natural biopolymer, which have been used for the preparation of hydrogels due to their unique properties. It includes hyaluronic acid, alginate, chitosan (CS), and cellulose [7] whose properties such as biodegradability, biocompatibility, non-toxicity, and low price preparation [8] make them suitable for many applications. In recent decades, CS has become one of the most widely used polysaccharides for the development of hydrogels. CS is produced by N-deacetylation of chitin, which is found in fungi and cell walls of algae, the exoskeletons of insects, mollusks, and crustacean. Its structure is comprised of randomly distributed  $\beta$ -(1 $\rightarrow$ 4)-D-glucosamine and N-acetyl-D-glucosamine units. Due to its properties, the use of CS has both environmental and practical importance demonstrating a high affinity towards several metal cations. [9] The presence of amino and hydroxyl groups in its structure makes it more reactive. Metal cations can be adsorbed by chelation on amino

groups of CS due to the free-electron doublet on nitrogen, and hydroxyl groups (especially in the C-3 position) may also contribute to sorption, [10] as shown in Figure 1.

Nevertheless, some disadvantages are associated with poor mechanical strength, elastic modulus, and tensile strength of CS. [11] Over the years, hydrogels have been modified to enhance their properties, and therefore expand their applications. Hydrogels can be tailored physically and chemically through crosslinking, grafting, impregnation, incorporating of hard fillers, blending, interpenetrating, and ion-imprinting methods to improve adsorption and mechanical properties. [11,12] To increase thermal, chemical stability, and mechanical resistance of hydrogels, the incorporation of inorganic materials has been studied. [13–15] Moreover, for the enhancement of the properties there are many different and unique nanoparticles employed for entrapment in hydrogel nanocomposite. [16]

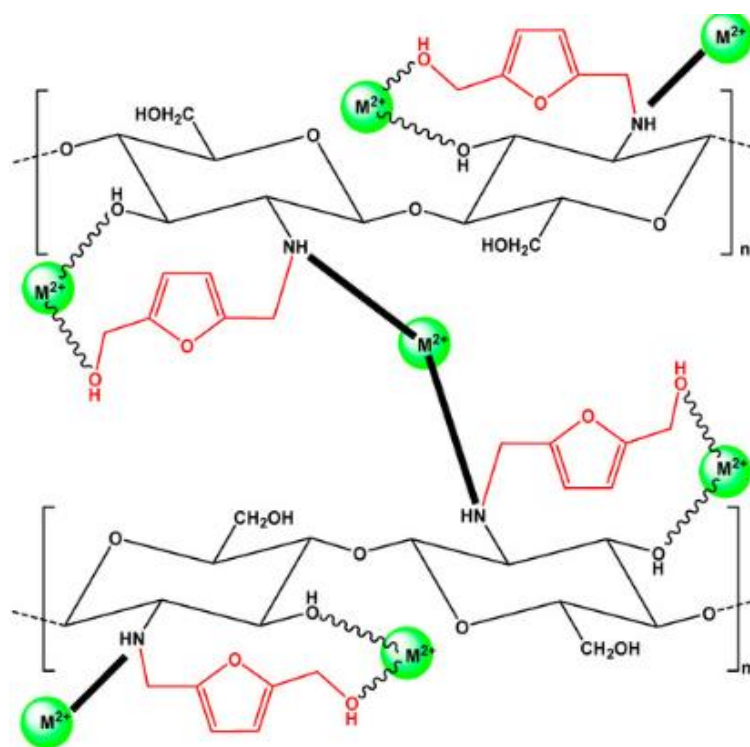


Figure 1. Adsorption mechanism of CS and metal ion. [17]

Nanocomposite hydrogels are defined as physically or chemically crosslinked polymer chains with different nanostructures. In the physical crosslinking, the networks of the structure are held together with hydrogen bonds or hydrophobic or ionic interactions. On the other hand, chemical crosslinking occurs through the formation of covalent bonds. [18] The main difference between covalent and physical crosslinking is

observed in the water solubility of the gels; the covalently crosslinked gels swell but do not dissolve in water, whereas physical gels eventually dissolve in water.

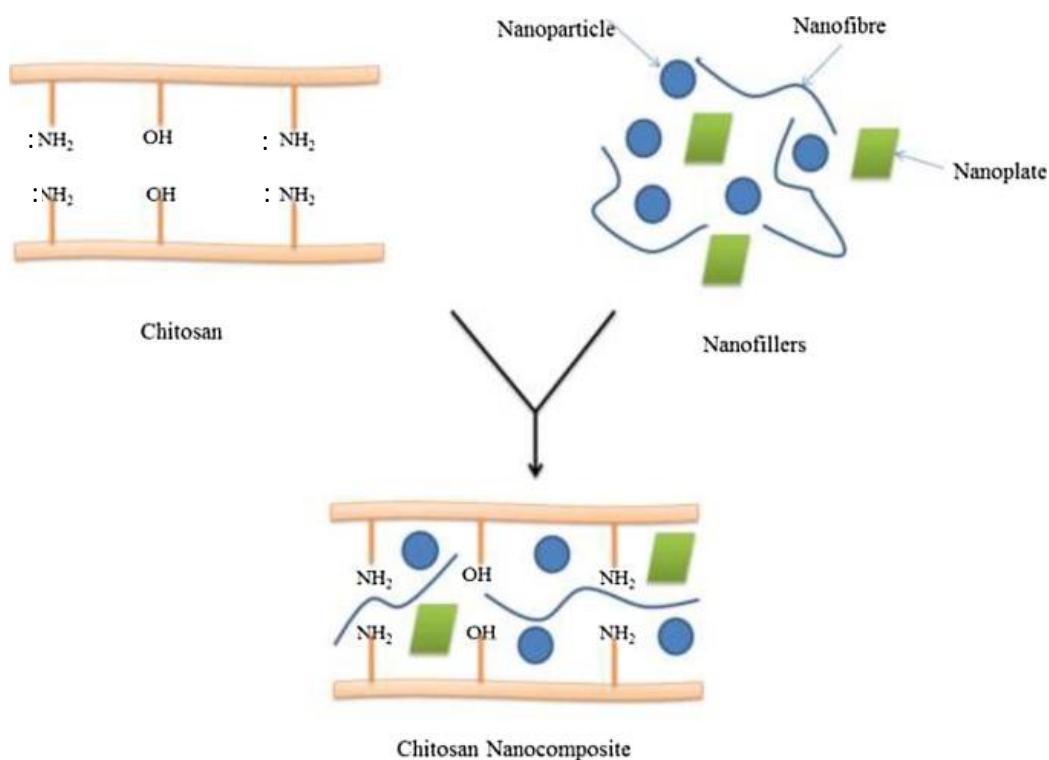


Figure 2. CS Nanocomposites structure taken from [10]

These nanocomposite hydrogels allow the enhancement of the intrinsic and extrinsic properties of the hydrogels matrix as a function of external stimuli due to the nanoparticles act as nano carrier within the matrix. [10] A schematic representation of the addition of nanostructures into the CS matrix is shown in Figure 2. This addition allows a broad application of the hydrogels as in catalysis, development of membranes used for separation, water purification, and various other biomedical applications. [19]

In this project the preparation (synthesis) of nanocomposites based on CS hydrogels / magnetite nanoparticles, among their morphology features and thermal stability evaluation are also presented. Results are compared with literature, for which an overview of the recent literature is also presented, as well as their application in wastewater treatment for the removal of metal ions and potentially toxic dyes.

## **2. Background**

### **2.1 Preparation of CS-based hydrogels**

Porous hydrogels are synthesized by various methods, such as freeze-drying [5, 17], cryogelation [21], and gas foaming [22]. The shape of the hydrogel depends on its application; it can be in the form of bead, film, and spheres; and, its shape conditions its application. Also, the incorporation of metal oxides nanocomposites could improve the CS hydrogels properties. Some researches involve cerium oxide cobalt oxide [19], graphene oxide [23], titanium oxide [24],  $\text{Fe}_3\text{O}_4$ , and  $\text{MnFe}_2\text{O}_4$  [25], among others. Depending on the pore size, CS-based hydrogel nanocomposites can be qualified as nanoporous (pores size below 10 nm), microporous (pore sizes in the 10 nm - 10  $\mu\text{m}$  range), and macroporous or super porous (pores size above 10  $\mu\text{m}$ ). [5] Consequently, a morphological characterization is required to know the hydrogel properties which provides suitable information for their application. Morphological analysis of the polymer allows a deep knowledge about the porosity, shape, size, and size distribution of the samples, which is crucial for the desired application of the hydrogels. [26] For the morphological analysis, several techniques are available, and among them, Scanning Electron Microscopy (SEM) is a technique widely used for polymer analysis. [27]

#### **2.1.2 Freeze drying technique**

Freeze drying has been widely used as a method for the production of porous hydrogels, consisting of three main steps: freezing, primary drying, and secondary drying. The first step consists of brought the polymer to low temperatures to transform into ice the part of the water that was bound. Then, in the primary drying step, free water from ice crystals is sublimated from the frozen sample. Finally, the secondary drying allows the water removal that was un-frozen. [24, 25]

The freeze-drying of native CS in acidic media leads to the formation of macroporous scaffolds. [28, 29] During the freezing process, the porous structure is produced by a separation between the water and the polymer. Ice crystal formation takes place, and after the drying step, they are removed to obtain a highly porous sample. Some researches claims that the porosity depends on water content, CS concentration, and also on freezing conditions (temperature, thermal gradient, and cooling rate). Therefore, the porous



structure of the material is associated with the freeze-drying experiment carried out. [5, 26,30]

The variables and conditions of the method influence the morphology of the polymer. For instance, Gutierrez et al. [31] studied the morphology of CS/PVA hydrogels by subjecting the hydrogels to different variables as the averaged molecular weight of the polymer, its concentration in the solution, and the freezing rate of the polymer solution where the conditions influence the pore diameter, surface area, and thickness of the material. By these means, the sample's porous channel size decreased with an increase of either the freezing rate or the molecular weight. It is stated that slow freezing rates allow the formation of large ice crystals, which ultimately template the microchannel structure. Meanwhile, fast freezing rates favor supercooling and, hence, impede the formation of large ice crystals, so that the micro channeled structure is scaled down. [31] This behavior was also reported by Memic et. al . [32] where the SEM images (Figure 3) shows that the freezing rate affect the pore structure of the hydrogels. [32]

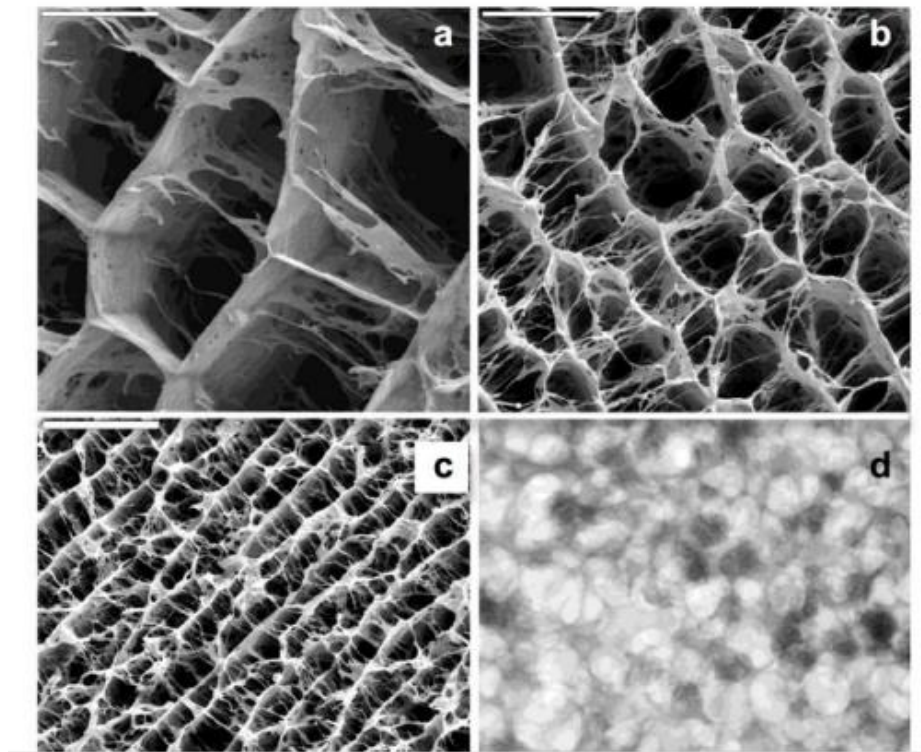


*Figure 3. SEM images of CS based hydrogels with calcium phosphate composition at different freeze-dried rates: (a) 0.7 mm/min; (b) 2.7 mm/min; (c) 5.7 mm/min. [32]*

The combination of methods influences the morphology of the polymer. Maji et al. [21] use a combined approach of high-speed stirring induced foaming and freeze-

drying method to develop macroporous scaffolds. The study reveals an evident effect of the high-speed stirring based foaming on the micro-architecture, pore size, and porosity of the scaffolds. Moreover, the ice crystal formation during the freezing process could have further contributed towards the dissolution of stabilized bubbles, which in turn might have resulted bubbles fusion, thereby, giving rise to a highly interconnected macroporous network with multimodal pore size distribution. [21]

### **2.1.3 Cryogelation**

Cryogelation is a simple method that allows the formation of inherently interconnected scaffolds by using freeze thawing. [32] In this context, the process consists of freezing the gelation solution, followed by the elimination of the solvent crystal via thawing (Figure 4). As a first step, the gel suspension is subjected to temperatures below the freezing point of the continuous phase (e.g water), allowing the crystallization of a large percentage of solvent, crosslinking, and polymerization. The rate of gel formation is affected by the concentration of the hydrogel monomers, oligomers, or polymers; also it is known as cryoconcentration. Subsequently, the thawing of the ice crystals in the polymer forming an interconnected porous cryogel network. [33] Besides, cryogelation is one of the easiest and least time-consuming techniques. [34]

By using this method, some CS-based hydrogels have been prepared, such as CS/clinoptilolite (CPL) biocomposite cryogels [35], cryogels based on methacrylic acid copolymers and CS [36], and CS/poly(ethyleneimine) (PEI) double network cryogels [37]. For instance, CS/CPL composite cryogels were prepared by cross-linking CS with glutaraldehyde (GA) in the presence of CPL particles, by using ice crystals as a template formed in a partially frozen state. Therefore, the pore walls of the CS network entrapping the CPL particles are formed within the non-frozen liquid microphase.

### **2.1.4 Gas foaming**

Gas foaming is a method used for the fabrication of macroporous hydrogels. This method uses a gas stream, at high pressure instead of organic solvents to produce the porous structure. During the procedure, the polymer networks are formed into the gas bubbles that have been caught into the polymer matrix. Active bubbling allows the formation of these gas bubbles within the solution. [34] Carbon dioxide (CO<sub>2</sub>) is the most commonly used dense gas because of its moderate critical properties, low toxicity, and

non-flammability. [38] However, hydrophilic and glassy polymers such as CS present low solubility in  $\text{CO}_2$ ; thus, the production of pores cannot be efficient. In this framework, to produce a porous structure in CS-based hydrogels,  $\text{NaHCO}_3$  or  $\text{N}_4\text{HCO}_3$  have been used as gas foaming agents. [39] For instance, super porous CS hydrogels (SPHs) were synthesized by combining microwave irradiation and gas foaming methods where  $\text{NaHCO}_3$  was employed as a blowing agent. SEM images indicate that the scaffolds had interconnected porosity and the sizes of pores were between 400-600  $\mu\text{m}$ . [40] Moreover, the use of  $\text{CO}_2$  as dense gas has been reported. Nanocellulose reinforced CS hydrogel was synthesized using a chemical cross-linking method by gas foaming where  $\text{CO}_2$  was employed. The study indicates a significant increase in the pore size of the hydrogels after using gas foaming. Atmospheric conditions present closed pore structures with around 100-300  $\mu\text{m}$  pore size. While using gas foaming, the pore size of the hydrogel significantly increased (more than 10-fold higher compared to the hydrogel formed at the atmospheric condition) with the formation of interconnected pore network structures. [41]

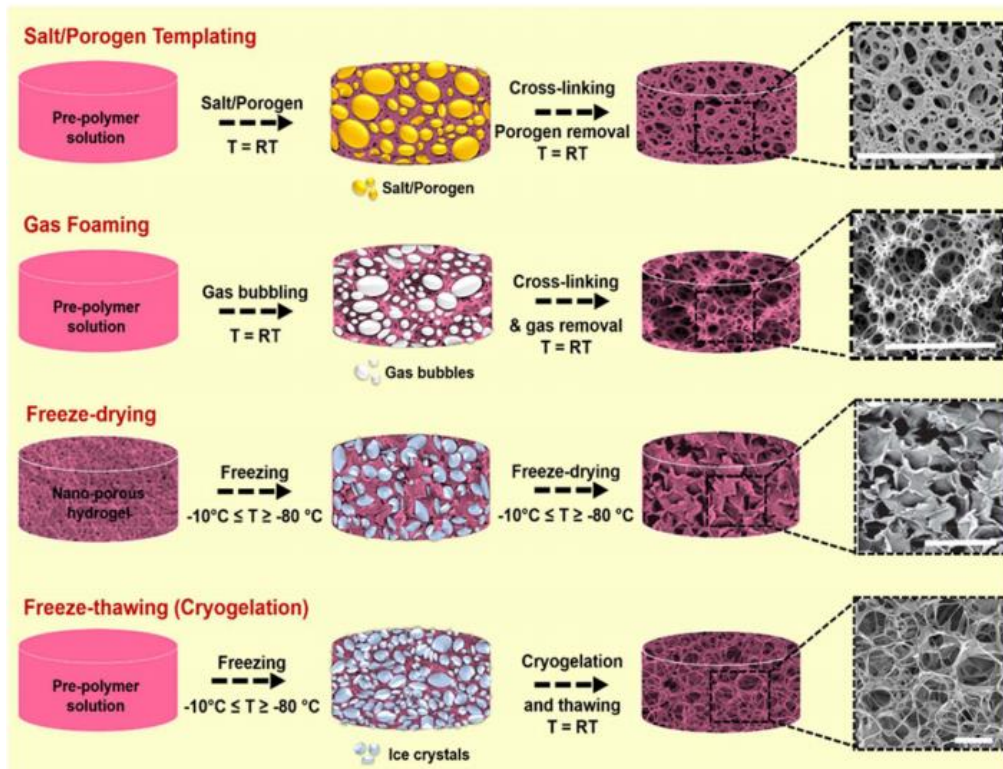


Figure 4. Several techniques used for the preparation of porous hydrogels. [36]

As mentioned previously, the method by which the sample is prepared had an influence the morphology. For instance, cryogels can present heterogeneous morphology, unidirectionally oriented pore, or two generations of pores, as shown in Figure 5.

Accordingly, a heterogeneous morphology with interconnected pores has been observed for the CS/CPL composite cryogels, with an average pore diameter of  $52 \pm 2 \mu\text{m}$  (Figure 5A). [35] Some researchers developed CS-based composites with lamellar structures by applying unidirectional frozen in liquid nitrogen ( $-196^\circ\text{C}$ ) of several aqueous mixtures or dispersions consisting of water-soluble polymers, inorganic particles, as shown in Figure 5B. [20] Moreover, 3D networks with two generations of pores have been developed by combining cryogelation and phase separation induced by the addition of n-butanol. SEM images are shown in Figure 5C indicate larger pores with sizes in the range of  $25\text{--}50 \mu\text{m}$  developed by cryogelation, and smaller pores between  $4\text{--}10 \mu\text{m}$  generated by phase separation. [42]

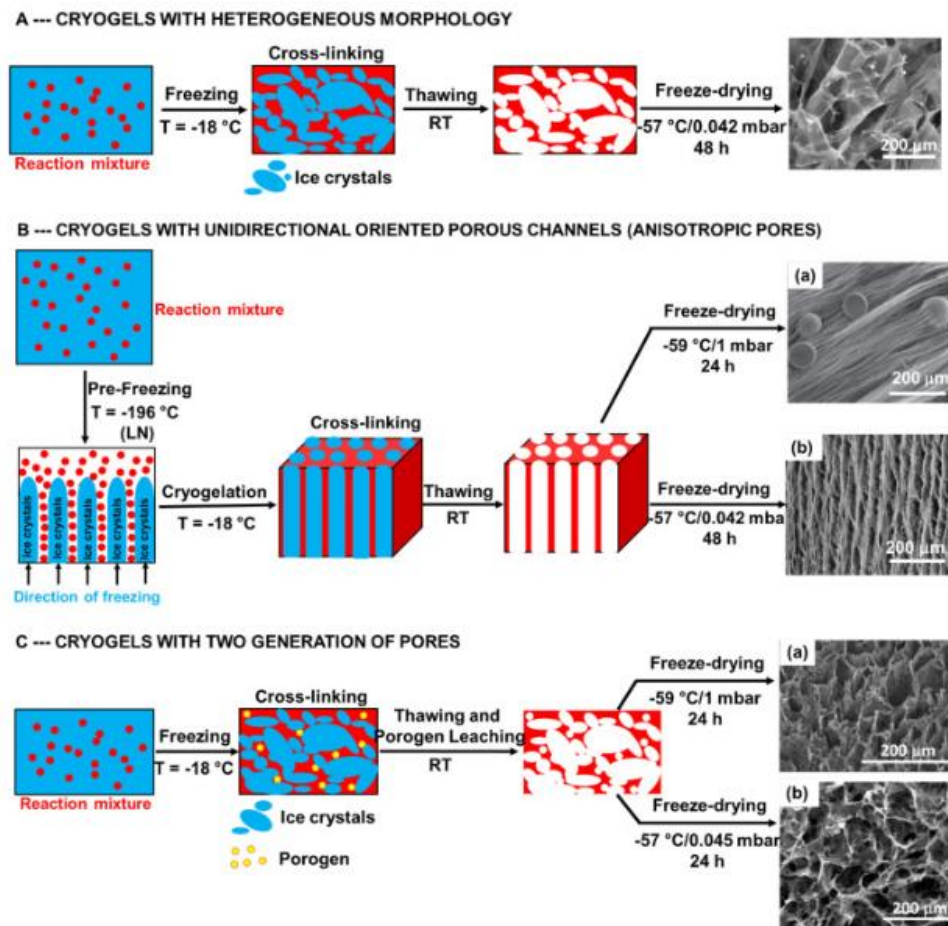


Figure 5. Preparation steps of CS-based cryogels with tailored porous morphologies. SEM images for cryogels with A) heterogeneous morphology, B) unidirectional oriented porous channels; and C) two generation of pores. [36]

Hydrogels generally possess poor functionality due to the amorphous structure, so the fabrication of order-structured hydrogels has drawn increasing attention. With ordered structures, the concentric multi-layers in CS hydrogels are alike the wood rings. [7]



Similar morphology was observed by Wang et. al. [43] which developed concentric-layered magnetic CS hydrogels which showed controlled layer numbers, layer thicknesses and dispersed MNPs. [43] Also, magnetic CS beads were synthesized by incorporating N,O-carboxymethyl CS-coated magnetic nanoparticles (NOCC-MNPs) into CS-citrate gel beads (CCGBs), the SEM images presented in Figure 6 indicate large porous. [44]

The morphology of CS/polyacrylamide (PAAm)/zeolite cryogels [45], CS/poly(vinyl amine) cryogels incorporating strong base anion exchanger microspheres, and CS/gelatin (GEL) scaffolds with aligned porous structures were studied. [17] As a result, the size between channels and the pore wall is being affected by several parameters such as crystallization speed, the molecular weight of CS, and the initial monomer or polymer concentrations, and the scheme of preparation. Kamal [24] coated pure CS and TiO<sub>2</sub>/CS nanocomposite on cellulose microfibrils mat (CMM) to develop adsorbent material for dye removal from wastewater. The morphological nature of MCMM being microfibrils in the range of 12~16 μm provided high surface area for CS and its TiO<sub>2</sub> nanocomposite adsorbents. By using Energy-Dispersive X-ray Spectroscopy was confirmed that the surface roughness was due to the TiO<sub>2</sub> nanoparticles. [24]

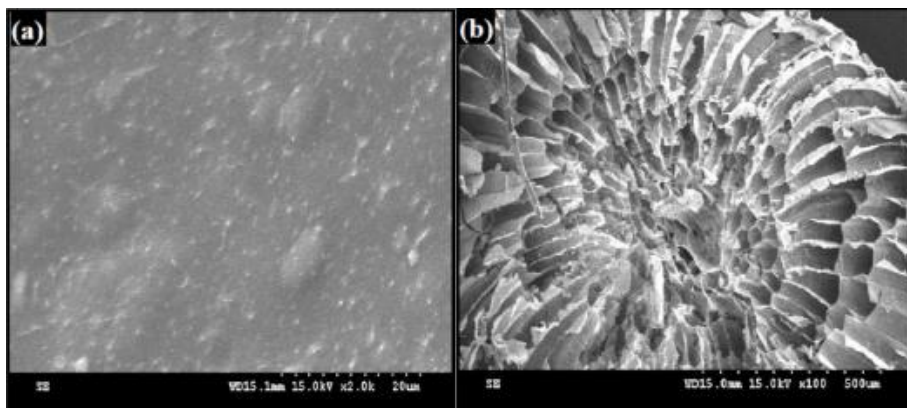


*Figure 6. SEM diagram micrographs of magnetic CS-citrate gel bead (CCGB): (a) surface, (b) cross-section. [44]*

Taghizadeh et al. [46] synthesized CS/AgCl/ZnO nanocomposite hydrogel beads. The morphology characterization reveals the formation of zinc oxide and silver chloride nanoparticles ranges from 20-40 nm. Moreover, the increase of AgCl in the polymer matrix causes no significant changes in the morphology of the nanocomposites. Nevertheless, it increases the organization of particles. The nanoparticles are well

dispersed on the CS surface SEM images of the beads show a non-uniform surface and splits which contribute with the adsorption of the pollutants and can be followed degradation after absorption of light. [46]

## **2.2 Properties of hydrogels**

The characteristics of a specific hydrogel are essential in selecting which materials are suitable for a given application. However, these are highly dependent on experimental conditions. With this combination of factors, it is imperative that hydrogel properties are determined and that they are measured under conditions that are as close to the in situ conditions as possible. [47] The features of the hydrogels, such as swelling, thermal stability, and mechanical properties, are discussed in the following section.

### **2.2.1 Swelling**

Hydrogels present the ability to respond to relatively small changes in stimuli with relatively significant changes in volume which promote their wide variety of applications. Swelling is a property that arises from this ability, and it is considered one of the most critical properties of hydrogels. The swelling behavior can be affected by the environmental conditions by which the polymer is subjected, process by which the solute diffuses into and is absorbed within the polymer. The constituents of polymer are forced apart, generating volume increase or swelling of polymer. [19]

The following equation can calculate the swelling of a polymer:

$$S_W \% = \frac{(W_s - W_d)}{W_d} \times 100 \quad (1)$$

where  $W_s$  and  $W_d$  represent the weight of the swollen and dry sample, respectively. [48]

Some researches state that the swelling of the hydrogels can be affected by the addition of nanocomposites as clays, inorganic particles, among others. For instance, the swelling behavior of CS, carboxymethylcellulose (CMC), and scleroglucan (SGL) by the addition of different amounts of Montmorillonite (MMT) has been studied. The results indicate a significant strong dependence of the swelling values with the amount of MMT; by this means, an increase in the MMT causes a decrease in the swelling capacity of the hydrogel. MMT within the hydrogel matrix affects the structure by producing stronger interaction between polymers and the mineral clay which generates a tighter one. It causes a reduction in the elasticity of the polymer chains and consequently the water holding

capacity of the hydrogels decrease [49] On the other hand, Nešović et al. [50] studied the effect on swelling with different concentrations of CS in silver nanoparticles/poly vinyl alcohol/CS/graphene (Ag/PVA/CS/Gr) hydrogel matrices. From the results, the swelling degree for PVA/0.5CHI/Gr was higher than for PVA/0.1CS/Gr, indicating higher sorption ability of hydrogels with higher CS content. [50] Moreover, the presence of silver nanoparticles increased the maximum swelling degree of hydrogels, especially in the case of the hydrogels with a higher content of CS. The AgNPs could contribute to the increase of the bound water content via the orientation of water dipoles and the formation of solvent cage around the nanoparticles. The equilibrium swelling degree as the maximum swelling degree reached equilibrium had greater values for hydrogels with a higher concentration of AgNPs and a higher concentration of CS. [50]

The swelling behavior can be affected by the pH at which the hydrogel is subjected. In this context, several types of research studied the pH response of the materials. [50] For example, the swelling kinetics of nanocomposites using a hydrogel based on a copolymer of acrylamide (AAM) and acrylic acid (AAc) as matrix and CS decorated CNT as reinforcement/modifier was studied by placed the samples for 24 h in buffers with different pH. As a result, nanocomposites with 5 and 10% of CNT-CH show a higher swelling percentage in a buffer solution with pH 8 and 10. At pH 2.2, the mesh is presented in a collapsed state due to the low value of pKa non-ionized carboxyl groups. On the other hand, at high pH, the electrostatic repulsion between the negatively charged carboxyl groups generate the swelling of the hydrogel network. So, the addition of significantly reduced the swelling in acidic conditions. [48] In agreement with this result, hydrogel nanocomposites were prepared by cross-linking of CS with 1,3,5-triazine-2,4,6-tribenzaldehyde in the presence of 0.1% and 0.3% (w/w) multi-walled carbon nanotubes (MWCNTs) and the swelling behavior was studied. Subsequently, the prepared hydrogels in the presence of 0.1% and 0.3% MWCNT-COOH displays a lower water absorption capacity than the CS-10% hydrogel, so that the swelling s with increasing MWCNT-COOH concentrations. [51]

### **2.2.2 Thermal Stability**

The thermal stability of hydrogels is affected by several parameters, such as the incorporation of nanocomposites. For instance, Caldas et al. [52] developed and characterized nanocomposite CS hydrogels with embedded poly (lactic-co-glycolic acid)

(PLGA) nanoparticles. The presence of the PLGA nanoparticles decreased the thermal stability of the nanocomposite compared to the pure CS hydrogel. The results demonstrated that the thermal stability of nanocomposites was slightly reduced due to the added nanoparticles. This slight change in the thermal stability of the nanocomposites compared to pure hydrogel might be due to the gelation by physical crosslinking that occurs through the emergence of reversible and transient junctions, and thus, they can be changed by physical conditions as temperature, for example. [52] Moreover, a thermogravimetric study of the commercial CS and the two freeze-dried CS nanoparticles (CTS-NPs) conjugates were conducted to reveal the variations in thermal degradability between the starting material and the composites. CS-based conjugates display almost identical thermogravimetric profiles and show a maximum degradation temperature at 281 °C. Although this value is slightly shifted to lower temperatures compared with the starting material (297 °C), the peak profile is similar to CTS's one. The new formulations experience a reduction in mass of 24% at low temperatures in contrast with the commercial CTS (9%), which could be mostly due to water content in the CTS sample. [53]

The data obtained from TGA experiments can be analyzed using the general equation of degradation as follows:

$$d\alpha / dt = Z (1 - \alpha)^n e^{-\frac{Ea}{RT}} \quad (2)$$

where  $\alpha$ ,  $t$ ,  $da/dt$ ,  $Z$ ,  $n$ ,  $Ea$ ,  $R$ , and  $T$  are the weight loss of the polymer undergoing degradation, the time at which  $\alpha$  is measured, the weight-loss rate, the frequency factor, the decomposition reaction order, the activation energy, the gas constant ( $8.3136 \text{ J mol}^{-1} \text{ K}^{-1}$ ), and absolute temperature ( $K$ ), respectively. The activation energy ( $Ea$ ) is the energy required for the onset of degradation, and the higher the activation energy, the higher the thermal stability of a polymer. On the other hand, the higher the activation energy, the higher would be the temperature dependency of the degradation process. The decomposition reaction order is represented by  $n$ , indicating the exponent of the reactants  $(1 - \alpha)$ , in the decomposition equation. Because the value of  $(1 - \alpha)$  is less than 1, higher values of  $n$  indicate lower rates of a decomposition reaction. Therefore, a thermostable system is characterized by higher values of  $Ea$  and  $n$  and vice versa. The dependence of the weight-loss rate on frequency factor ( $A$ ) is such that by increasing  $A$ ,



the weight-loss rate increases, but  $A$  has no effect on the temperature dependency of the degradation process. [85–87]

To determine the activation energy ( $Ea$ ), the reaction order ( $n$ ) and the pre-exponential factor ( $A$ ), the Friedman Method was used, which is a general method with direct application to the degradation kinetics. This method is based on the comparison of the rates of weight loss ( $d\alpha / dt$ ) for a fractional weight loss  $\alpha$ . [57] This method uses the following differential equation:

$$\ln (d\alpha/dt) = \ln A + n\ln(1 - \alpha) - \frac{Ea}{RT} \quad (3)$$

Conveniently, the experimental parameter  $\beta = dT / dt$ , representing the heating rate of thermogravimetric experiments, is introduced in the equation 3. In this way, the linearization applied to this expression is the following:

$$\ln (d\alpha / dT) = \ln A/\beta + n\ln(1 - \alpha) - \frac{Ea}{RT} \quad (4)$$

In this method, it is necessary to work in a range of degrees of advance to which the linear adjustment is adequate. In such a way that to obtain a good linear fit, it is analyzed in a graph of  $(d\alpha / dT)$  vs. the interval before the maximum point of the hood where the behavior is linear. From equation (4) it is possible to determine the value of the apparent activation energy for each speed considered at the slope of the graph of  $\ln (d\alpha / dT)$  vs.  $1 / T$ . Once the value of  $Ea$  has been calculated, it is possible to determine the order of reaction and the pre-exponential factor representing the values of  $[\ln (d\alpha / dT) + Ea / RT]$  versus  $\ln (1 - \alpha)$ . This fit should give a straight line whose slope is the reaction order and whose ordinate at the origin is  $\ln (A / \beta)$ . [57]

### 2.2.3 Mechanical properties

Mechanical properties of the hydrogels are considered an important factor to take into account to design and determine the particular applications for these polymers. [58] As an advantage, the skeleton of CS is composed of amino and hydroxyl groups, which allow the formation of hydrogen bonds and interactions with groups from molecules or polymer chains such as amide, hydroxyl, and epoxy group. These characteristics proper of CS allow the enhancement of the mechanical properties of hydrogel material. [59] Nevertheless, one of the main problems with most of the hydrogels, especially CS hydrogels, is related to its lack of stiff, tough, and stretchable caused by the intrinsic

heterogeneity of the network structure and lack of efficient energy-dissipation mechanisms. [10] Consequently, it has a significant impact on the suitability of the hydrogels for being applied in specific applications. Several methods and strategies have been widely studied and developed to enhance the mechanical performances of hydrogels, and it includes the constructing multiple-network structures (double-network and an interpenetrating polymer network) the introduction of novel crosslinkers (chemical and physical crosslinkers), dynamic interactions (ionic bonds, the interaction between the cationic and anionic group and hydrogen bonds) and nanoparticle reinforcement. [59] For instance, Wu et al. [60] reported double network hydrogels containing short-chain CS prepared via a universal soaking strategy, in which CS was found to impart excellent mechanical properties to the composite hydrogels. [60]

Several theories have been employed to understand the mechanical behavior of hydrogels; the most used are the theories of rubber elasticity and viscoelasticity, which allow a better understanding. These theories are based on the time-independent and time-dependent recovery of the chain orientation and structure, respectively. [61] By using methods to describe the mechanical behavior, it is possible to analyze the polymer structure and determine the effective molecular weight between crosslinks as well as to elucidate information about the number of elastically active chains and cyclization versus crosslinking tendencies. It is also possible, and sometimes necessary, to use theories to extrapolate mechanical properties to conditions in which the material may be used. In many instances, it is not possible to test the hydrogel under the exact circumstances in which the device is used. [47]

The mechanical strength of porous CS-based composite hydrogels was mainly investigated by tensile and compression tests. The specific parameters which describe the mechanical properties of hydrogels such as Young's modulus, tensile strength, and yield strength are usually obtained from the stress-strain charts. [36]

The mechanical elasticity curve for hydrogels with different loads of CNT-CH was studied. The analysis was performed by analyzing the modulus of elasticity of the composites with different CNT content. As a result, there is a tendency in the behavior of nanocomposites with the content of CNT, by its means, it changes from elastic, for low loads of CNT (hydrogel-CNT1%) that is similar to pure acrylamide hydrogel, towards a more rigid and resistant to compression hydrogel for higher loads (hydrogel-CNT5%, hydrogel-CNT10%). [48] Moreover, A new multi-structural network design for

mechanically enhancing graphene oxide (GO) filled CS-based hydrogel nanocomposites were developed. The designed multi-structural hydrogel network shows a relatively dense structure with surrounding polymer chains at the local zone of self-assembled GO-CS units resulting in the mechanical enhancement is composite system, hydrogen bonding and electrostatic attraction between the polycationic CS and the negatively charged GO sheets are mainly favorable to the effective stress transfer. [62]

### **2.3 Application of CS-based Nanocomposite Hydrogels for pollutant removal**

Nowadays, pollution from industries such as heavy metal ions, pesticides, dyes, various microorganisms, and solid particles is a serious concern due to the negative effects it brings to the environment and human health. An ecological solution needs to be developed to overcome this problem. Recently, the addition of composites into CS-based hydrogels such as metals, metal oxides, magnetite, and bimetal compounds has been increasingly studied as an alternative adsorbent in water treatment, allowing the adsorption of heavy metals and dyes from wastewater. [63, 64] Owing to the presence of free amino groups in CS structure, it can serve as an effective adsorbent and coagulant, reducing the number of suspended solids, metal ion chelators, or binding dye. [65]

Kinetics studies are of great importance for a practical application of heavy metal ion removal, which helps to understand the mechanism of adsorption and its potential rate-limiting steps. Also, information on the kinetics of heavy metal uptake is required to select the optimum condition for the full-scale batch metal removal process. [66] In general, the overwhelming majority of kinetic studies are implemented in batch experiments using linear or non-linear regression to ascertain the best-fitting kinetic model. The three most common kinetic models, namely the pseudo-first-order kinetic model (PFO), the pseudo-second-order kinetic model (PSO), and the intra-particle diffusion model, have been widely used for the process of metal ion removal on MCS. These models provide valuable information about the mechanism that controls the adsorption process. [67]

#### **2.3.1 Dye removal**

Synthetic dyes are organic compounds that are widely used in industries such as textiles, paper, plastic food, or cosmetics. These pollutants are commonly found in wastewater as a serious threat to human health and the environment due to their complex

aromatic structure and synthetic origin that make removal difficult. They are produced on a large scale. The exact number of dyes produced in the world is uncertain, but it is estimated that there are 100,000 dyes available. Many of them are known to be non-biodegradable, toxic and carcinogenic. [58,60]

Based on their chemical structure, dyes can be categorized as anionic (direct, acid, and reactive dyes), cationic (basic), and non-ionic (disperse). Moreover, there are many structural varieties, such as acidic, disperse basic, azo, diazo, anthraquinone-based, and metal complex dyes. The major classes of synthetic dyes and pigments are azo and anthraquinone colorants. [68]

The most common dyes found in wastewater are Methylene Blue (MB), Reactive Black 5 (RB), Methyl Orange (MO), Basic Blue (BB), Congo Red (CR) Dye, Anthraquinone dye, among others. Methylene blue is a sulfur-containing heterocyclic aromatic cationic dye. This water-soluble dye is widely used in textile, printing, and food industries for dyeing cotton, silk, and wool. For the removal of MB, various porous composite sorbents based on CS have been developed and tested. For instance, CS-gelatin based hydrogel was modified by incorporating zirconium (IV) selenophosphate cation exchanger nanoparticles. The alteration within the polymer matrix increases the dye removal capacity since the nanoparticles enhance the surface area of the nanocomposite as well as provide some additional binding sites for the adsorption of MB molecules. [69] The photocatalytic degradation of MB via CS/AgCl/ZnO nanocomposite hydrogel beads system has also been reported. The research consists of the direct photolysis of MB on the beads under light illumination. As a result, the photolysis of MB is slow without a photocatalyst under light illumination. The photocatalytic degradation of MB solution in the presence of CS/AgCl/ZnO beads under light illumination is higher than that of direct photolysis, indicating that CS/AgCl/ZnO beads are active under visible light irradiation. The decrease of MB concentration in the presence of CS/ZnO under visible light is low, only 34% of MB was degraded in 135 min, which is associated with the bandgap of ZnO is 3.16 eV, and it can absorb UV light effectively. [46]

Moreover, the addition of magnetic nanoparticles within the polymer matrix allows separation using magnetic fields and, consequently, the recycling of the gel particle. For instance, Abd-Elhakeem et al. [70] have prepared CS-coated magnetite nanoparticles and used them as adsorbent, chelating agents, or bactericidal agents to remove organic contaminants, heavy metals, and bacteria from water. In their research,

they find that the adsorption capacities of the different pollutants considerably increased with CS-magnetite nanoparticle concentration. The highest affinity was observed for petroleum impurities, where 1 g of CMNP removed about 98 % from it. At the same time, the lowest capacity was recorded by heavy metals. [70] Moreover, ampholytic CS/carrageenan (CS/CRG) microspheres modified with Fe<sub>3</sub>O<sub>4</sub> nanoparticles have been synthesized, and adsorption test was performed. Subsequently, the microspheres exhibited high adsorption capacity towards cationic and anionic dyes and heavy metal ions. The microspheres present a strong electrostatic and chelating affinity that makes it suitable for the efficient adsorption of water pollutants. Additionally, they were modified with Fe<sub>3</sub>O<sub>4</sub> nanoparticles to allow magnetic separation. Developed microspheres are environmentally friendly since they can be easily recycled, reused, and biodegraded in soil. [71] For the removal of Congo Red from aqueous solution, CS/poly(vinyl alcohol) (PVA)/Fe<sub>3</sub>O<sub>4</sub> hybrid gel particles were prepared using an instantaneous gelation method. Such hybrid gel particles were developed as low-cost, recyclable biomaterials for the removal of Congo Red from aqueous solution, in which case the inclusion of the magnetic NPs allows the separation and recycling of the gel particles using magnetic fields. The results show that when compared to PAAm/CS hydrogels, PAAm/CS/ Fe<sub>3</sub>O<sub>4</sub> hydrogels can adsorb MB with higher adsorption capacities. [72]

Crystal violet (CV) is one of the most toxic organic dyes, thus there is a critical need to remove it from wastewater before discharging into the environment. Some researches have been developed hydrogels to remove this dye from water. [73] For instance, magnetic nanocomposite hydrogels using an in-situ synthesis of carboxymethyl CS/poly(acrylamide) (CMC-PAM) hydrogels in the presence of Fe<sub>3</sub>O<sub>4</sub> - montmorillonite nanoparticles (m-MMT) via crosslinking graft copolymerization were developed. The magnetic nanocomposite CMC-PAM hydrogels (m-CMC-PAMH) were used to remove and separate CV as a cationic dye from aqueous solutions using the electrostatic interactions between the hydrogels and CV molecules. The adsorption test demonstrates that the introduction of m-MMT has improved the amount of adsorption in acidic environments. [74]

Some of the lately published results obtained at the sorption of various dyes on the porous composite sorbents based on CS are summarized in Table 1.

Table 1. Results reported in literature obtained for dye removal from CS-based hydrogel nanocomposites.

<i>Hydrogel Structure</i>	<i>Dye</i>	<i>mg/g</i>	<i>Kinetics</i>	<i>Isotherm</i>	<i>Ref.</i>
<i>(m-CS/PVA HBs)</i>	<i>CR</i>	<i>470.1</i>	<i>PSO</i>	<i>Langmuir</i>	[72]
<i>Magnetic CS/carrageenan composite</i>	<i>CR</i>	<i>212.84</i>	<i>PSO</i>	<i>Langmuir</i>	[71]
	<i>MB</i>	<i>124.84</i>	<i>PSO</i>	<i>Langmuir</i>	[71]
<i>PAAm/CS/magnetite hydrogels</i>	<i>MB</i>	<i>160.3</i>	<i>PSO</i>	<i>Langmuir</i>	[15]
<i>Magnetic CMC-PAM hydrogels</i>	<i>CV</i>	<i>72.4</i>	<i>PSO</i>	<i>Langmuir</i>	[74]
<i>Magnetic CS/carrageenan</i>	<i>MB</i>	<i>123.1</i>	<i>PSO</i>	<i>Langmuir</i>	[75]
<i>CS-lignin-titania</i>	<i>BB</i>	<i>15.8</i>	<i>PSO</i>	<i>Langmuir</i>	[76]
<i>Nickel ferrite nanocomposite/functionalized CS</i>	<i>MO</i>	<i>551.2</i>	<i>PSO</i>	<i>Langmuir</i>	[77]
	<i>CR</i>	<i>274.7</i>	<i>PSO</i>	<i>Langmuir</i>	[77]
<i>CS-lignin-titania</i>	<i>BB</i>	<i>15.8</i>	<i>PSO</i>	<i>Langmuir</i>	[76]

### 2.3.2 Potentially toxic metals

Organic polymers as CS, PVA, among others have been incorporated inorganic nanomaterials to enhance the adsorption for various heavy metals present in wastewater. Some researches involve inorganic adsorbents as activated carbon, zeolite, magnetite, and graphene oxide (GO). CS has been widely studied for the removal of both cations and anions and it has demonstrated great performance for this application. Metal adsorption can be affected by the pH of the solution since this factor affect both the ionization state of the metal ions and the availability of the functional groups of the sorbent. Herewith, the cations can be adsorbed onto the amine groups present in the CS structure in neutral solutions. Otherwise, the anion groups such as dichromate and chromate can be removed by ion exchange in acidic solutions due to the protonation of amine groups. [78]

Within metal ions found in wastewater, some researchers have been focused on  $\text{Cu}^{2+}$ ,  $\text{Co}^{2+}$ , and  $\text{Ni}^{2+}$ . Although they are essential for living organisms, there are permissible limits for these ions in water due to the consequence that it can be associated with. For instance, exciding the allowable concentrations of 2.0 mg/L for  $\text{Cu}^{2+}$  can produce several symptoms such as nausea, vomiting, gastrointestinal illness, muscle pain, liver poisoning,

kidney failure, and Wilson's disease.  $\text{Ni}^{2+}$  has a tolerance limit of 0.01 - 0.02 mg/L in drinking water. Still, the exposition to high concentrations may affect human health by causing dermatitis, gastrointestinal disturbances, liver or kidney failure, dysfunctions of the central nervous system, cancer of the lungs and bones, and may have mutagenic effects. In the same way, exceeding the tolerance limit of  $\text{Co}^{2+}$  concentration in water, food, and as radioactive cobalt in the environment may cause low blood pressure, paralysis, diarrhea, lung irritation, and bone defects. [79]

For the removal of  $\text{Cu}^{2+}$ ,  $\text{Ni}^{2+}$ , and  $\text{Co}^{2+}$  cryogels biocomposites were synthesized by the dispersion of some starches-g-PAN in CS solution where glutaraldehyde (GA) and poly(ethylene glycol diglycidyl ether) (PEGDGE) were used as crosslinkers to stabilize the cryobeads. From this research was concluded that the botanical origin of starch influences the sorption capacity at equilibrium. The cryogels show a high adsorptivity for the metal ions, in which the  $q_m$  values can be placed in the order:  $\text{Cu}^{2+}$ ,  $\text{Ni}^{2+}$ ,  $\text{Co}^{2+}$  increased with the decrease of the hydrated cation radius. [80]

Some of the lately published results obtained at the sorption of various metal ions on the porous composite sorbents based on CS are summarized in Table 2.

Table 2. Results reported in literature obtained for dye removal from CS-based hydrogel nanocomposites.

<b>Hydrogel Structure</b>	<b>Metal</b>	<b>mg/g</b>	<b>Kinetics</b>	<b>Isotherm</b>	<b>Ref.</b>
<i>Cs/CDTA/GO hydrogels</i>	<i>Cr<sup>6+</sup></i>	166.9 8	<i>PSO</i>	<i>Langmuir</i>	[78]
<i>Magnetic CS/carrageenan composite</i>	<i>Cr(III)</i>	20.19	<i>PSO</i>	<i>Langmuir</i>	[71]
	<i>Cu(II)</i>	12.33	<i>PSO</i>	<i>Langmuir</i>	[71]
<i>CINs</i>	<i>As(III)</i>	267.2	<i>PSO</i>	<i>Langmuir</i>	[81]
<i>α-MnO<sub>2</sub>-APTS/CS nanocomposites</i>	<i>Pb(II)</i>	-	-	-	[82]
<i>CS and starches-g-PAN hydrogel</i>	<i>Co(II)</i>	100.6	<i>PSO</i>	<i>Langmuir, and Sips</i>	[58]
	<i>Ni<sup>2+</sup></i>	83.25	<i>PSO</i>	<i>Langmuir, and Sips</i>	[58]
	<i>eCo<sup>2+</sup></i>	74.01	<i>PSO</i>	<i>Langmuir, and Sips</i>	[58]



### **3. Problem Statement**

In recent years, water pollution has become one of the major threats to human health with the increase in industrial activity. Metal ions and organic pollutants are of significant concern due to the environmental and health problems that it brings. The adsorption method is one of the most chosen to overcome this issue because of its simplicity, non-toxicity, cost-effectiveness, and local availability to remove toxic heavy metals from the aqueous medium. CS-based hydrogels nanocomposites are a suitable option for potentially toxic metals and dyes removal from water and wastewater treatments.

## **4. Objectives**

### **4.1 General Objective**

To obtain CS hydrogels with magnetite nano particles for the wastewater treatment.

### **4.2 Specific Objectives**

1. To synthesize magnetic CS hydrogels by in situ co-precipitations crosslinked with glutaraldehyde by two methods: drip and solvent evaporated method.
2. To characterize the obtained hydrogels and evidence their morphology, thermal stability, and presence of magnetite nanoparticles.
3. To provide information about the recent development on the application of CS-based hydrogels nanocomposites as adsorbents in the removal of dye and potentially toxic metal ions in water.

## 5. Methodology

### 5.1 Materials

Low molecular weight CS with a deacetylation degree of 76 % (CAS number: 9012-76-4), Glacial Acetic Acid (100%) and Glutaraldehyde (25 v/v % water solution) were purchased by Sigma Aldrich, Sodium hydroxide (1 mol/L) were supplied by Riedel de Haen, Iron sulphate heptahydrate ( $\geq 98\%$ ) and chloride hexahydrated ( $\geq 98\%$ ) were supplied by Panreac. All the reagents were used without further purification.

### 5.2 Experimental Description

The hydrogels were prepared by two methods: Drip and solvent evaporated.

#### 5.2.1 CS solution

The solution of CS was prepared by pouring 1 g of CS into 0.5 mL of acetic acid (99.5 wt %,  $d = 1.05 \text{ g/mL}$ ) and 49.5 mL of distilled water. Then it was stirred overnight to let the CS dissolves completely.

#### 5.2.2 Iron CS solution

Iron sulfate heptahydrate and iron chloride hexahydrate salts were dissolved into the solution of CS previously prepared, resulting in an orange solution.

#### 5.2.3 Drip Method

##### 5.2.3.1 CS-based hydrogels beads

For the samples without crosslinker, 4 mL of CS solution was dropped slowly by using a 0.6 mm syringe needle into 25 mL of NaOH 1M solution; then, the formed beads were saved at room temperature for 24 h without stirring and then washed several times in water to remove alkaline and stored in distilled water. The same procedure was repeated by using an iron CS solution; in this case, the beads turn black due to the formation of magnetite. For the crosslinked samples, 2 g of hydrogel beads were collected and kept for 24 hours in 200 mL of glutaraldehyde (GLA) aqueous solutions of 0.35% and 0.75%. The beads were finally washed to remove non-reactant GLA and collected in distilled water. The schematic preparation of hydrogels beads prepared by the drip method is shown in Figure 7, and their corresponding nomenclature samples are presented in Table 3, given by  $Q_D X$ ,  $Q_D M$  and  $Q_D X M$ . In

the used codes, the presence of glutaraldehyde is denoted by the X being the subscript % the amount of it, while M represents the presence of magnetite nanoparticles.

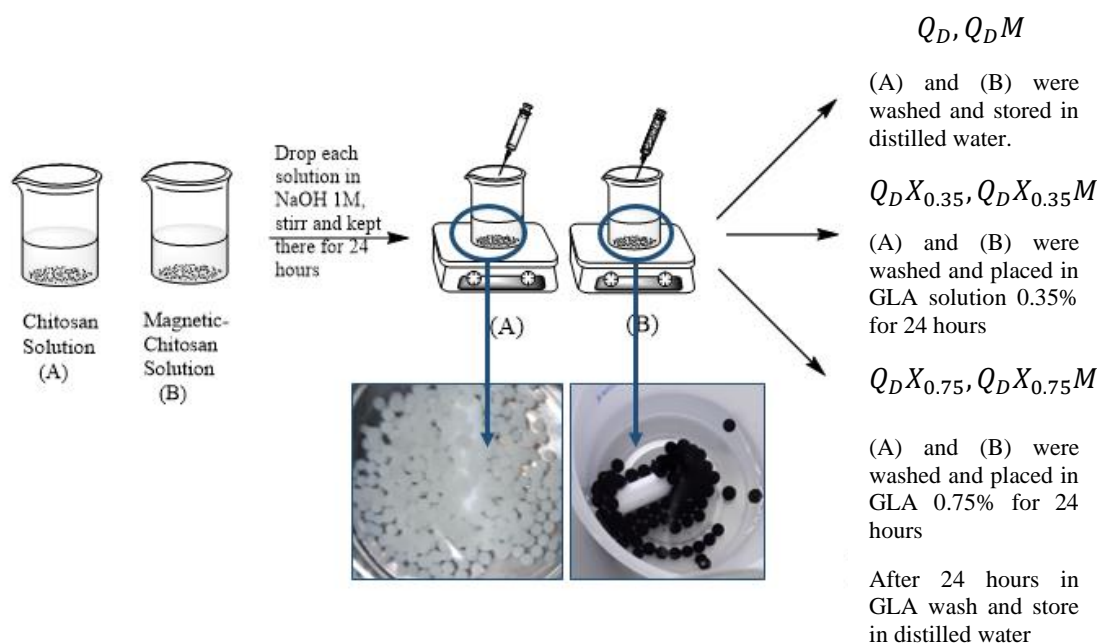


Figure 7. Schematic representation of hydrogels beads preparation by the drip method.

## 5.2.4 Solvent Evaporated Method

### 5.2.4.1 CS-based hydrogels beads

For the preparation of the un-crosslinked samples, 2 mL of CS solution and iron CS solution were placed in silicone molds about an hour until it takes a jelly consistency, then were placed in 20 mL of NaOH 1 M solution. After 24 hours, the gels were washed to remove the excess alkaline solution. Finally, the gels were stored in distilled water. For the crosslinked samples, 2mL of CS solution was placed in a beaker; then, 0.28 mL and 0.60 mL of glutaraldehyde (25 v/v%) was added to obtain a final concentration of 0.35 and 0.75 v/v%, respectively. The solutions were placed in silicone molds until it takes a jelly consistency, then were placed in 20 mL of NaOH 1 M solution. After 24 hours, the gels were washed to remove excess alkaline solution and stored in distilled water. The same procedure was employed by using an iron CS solution. The schematic representation for the preparation of hydrogels by the solvent evaporated method is shown in Figure 8, and their corresponding nomenclature samples are presented in Table 3, whose codes were described above.

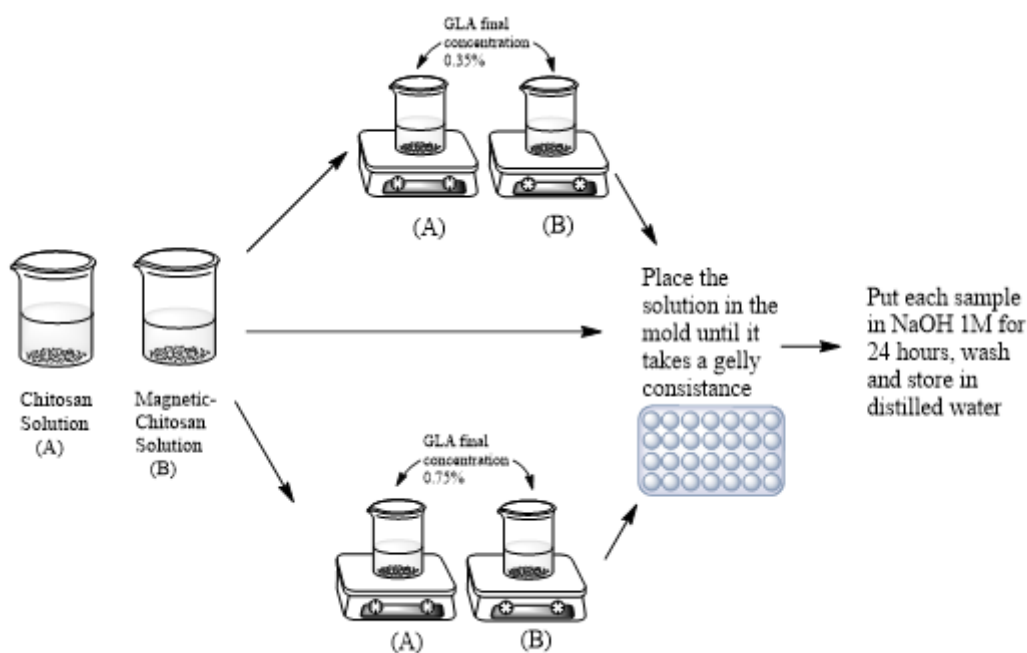


Figure 8. Schematic preparation of hydrogel beads prepared by the solvent method.

Table 3. Nomenclature of CS-based hydrogel beads prepared in this work.

<i>Samples</i>	<i>Preparation Method</i>	<i>% Glutaraldehyde</i>	<i>Magnetite</i>
$Q_D$	<i>Drip Method</i>	-	×
$Q_D X_{0.35}$	<i>Drip Method</i>	0.35%	×
$Q_D X_{0.75}$	<i>Drip Method</i>	0.75%	×
$Q_D M$	<i>Drip Method</i>	-	✓
$Q_D X_{0.35} M$	<i>Drip Method</i>	0.35%	✓
$Q_D X_{0.75} M$	<i>Drip Method</i>	0.75%	✓
$Q_{SE}$	<i>Solvent Evaporated Method</i>	-	×
$Q_{SE} X_{0.35}$	<i>Solvent Evaporated Method</i>	0.35%	×
$Q_{SE} X_{0.75}$	<i>Solvent Evaporated Method</i>	0.75%	×
$Q_{SE} M$	<i>Solvent Evaporated Method</i>	-	✓
$Q_{SE} X_{0.35} M$	<i>Solvent Evaporated Method</i>	0.35%	✓
$Q_{SE} X_{0.75} M$	<i>Solvent Evaporated Method</i>	0.75%	✓

The cross-linked of the CS samples and the formation of nanoparticles of magnetite was evidenced by the analysis of samples by different characterization techniques. These analyses allowed the evaluation of some of their morphological and chemical feature.

### **5.3 Scanning Electron Microscope (SEM)**

The morphological study of prepared samples was performed by Scanning Electron Microscopy (SEM) with a Hitachi TM3030 microscope. The hydrogel samples were quickly introduced in liquid nitrogen and further lyophilized with a freeze dryer system under vacuum for 24 h until the water is sublimed. To observe the internal morphology, the freeze-dried samples were fractured and coated with gold for conductance under vacuum by a sputter. Analysis of the pore structure was done using TM3030 software.

### **5.4 Thermogravimetric Analysis (TGA)**

Thermogravimetric measurements were performed by using the Q500 thermogravimetric analyzer from TA instruments. Non-isothermal experiments were performed in the temperature range from 30°C to 600 °C at a heating rate of 10 °C/min on the hydrated and freeze-dried samples. The thermal stability was evaluated using derivative plots of derivative weight (%/ °C) vs. temperature (°C).

### **5.5 X-Ray Diffraction (XRD)**

X-ray powder diffraction patterns were collected by using a Philips X'pert PRO automatic diffractometer operating at 40 kV and 40 mA, in theta-theta configuration, secondary monochromator with Cu-K $\alpha$  radiation ( $\lambda = 1.5418 \text{ \AA}$ ) and a PIXcel solid state detector (active length in  $2\theta$  3.347°). Data were collected from 5 to 70°  $2\theta$ , step size 0.026° and time per step of 150s at RT. 1° fixed soller slit and divergence slit giving a constant volume of sample illumination were used.

The measurements were made in the Institute of Polymeric Materials "POLYMAT" in San Sebastián – Spain.

## 6. Results and Discussion

### 6.1 Morphology of CS-Based Hydrogel Nanocomposites

In the present work, magnetic CS hydrogels have been prepared by in-situ co-precipitation. The images obtained for the surface and external surface of the studied samples are shown in Figure 9 and 10, showing the different conditions through the figures A, B, C, D, E, and F for each one of them, in addition, complementary images are presented in the Figures 1A, 2A, 3A, and 4A presented in the annexes. SEM images of the CS-based hydrogels prepared by the drip method (Figure 9) illustrate that the samples are porous beads with a more regular surface and pores size in the range of 0.34 – 0.95  $\mu\text{m}$  which can be qualified as microporous; on the other hand, the samples prepared by solvent evaporated method present irregular and elongated shape with a pore diameter in the range of 35- 80  $\mu\text{m}$  which can be qualified as macroporous hydrogels. In this case the preparation affects the size of the pores, much smaller sizes are obtained by dripping. This may be due to the fact that due to the precipitation process a much more compact structure is formed, where the solvent leaves the structure leaving only the polymer (and the magnetite when applied), however in the case of evaporation of the solvent the solvent remains within the network and, as it evaporates, creates channels and pores that are noticeably larger. Figure 9 indicates that the ( $Q_D$ ) average porous size diameter (0.95  $\mu\text{m}$ ) of natural CS is larger than the diameters of crosslinked samples  $Q_D X_{0.35}$ , and  $Q_D X_{0.75}$  with (0.4 $\mu\text{m}$ ) and (0.34 $\mu\text{m}$ ), respectively. The same tendency is observed for the samples prepared by the solvent evaporated method, where the increase in the amount of GLA concentration implies a decrease in the diameter porous size.

Figure 10 indicates that crosslinked samples prepared by solvent evaporated method present different size distribution where the small pore size diameter for  $Q_{SE} X_{0.35}$  are 40  $\mu\text{m}$  and larger ones around 80  $\mu\text{m}$  and  $Q_{SE} X_{0.75}$  sample with tiny pores of 30  $\mu\text{m}$  and larger ones around 45.6  $\mu\text{m}$ . On the other hand, although the addition of magnetite preserves the porous network structure of the hydrogels, it influences the pore diameter where the average porous size of the samples that present magnetite is larger. By these means, the average pore diameter of magnetic samples prepared by the drip method is around 26  $\mu\text{m}$ . The images showed in all cases well-formed particles with regular shapes and well defined porous. Nevertheless, being the average porous size of the cross-linked magnetic samples ( $Q_D X_{0.35} M$  and  $Q_D X_{0.75} M$ ) was similar; this outcome

indicates that the increase in the concentration of crosslinker did not alter the size of the diameter pores. From SEM was not possible to observe the magnetite particles. Therefore, the presence of magnetite nanoparticles is confirmed by XRD which will be discussed in the next section.

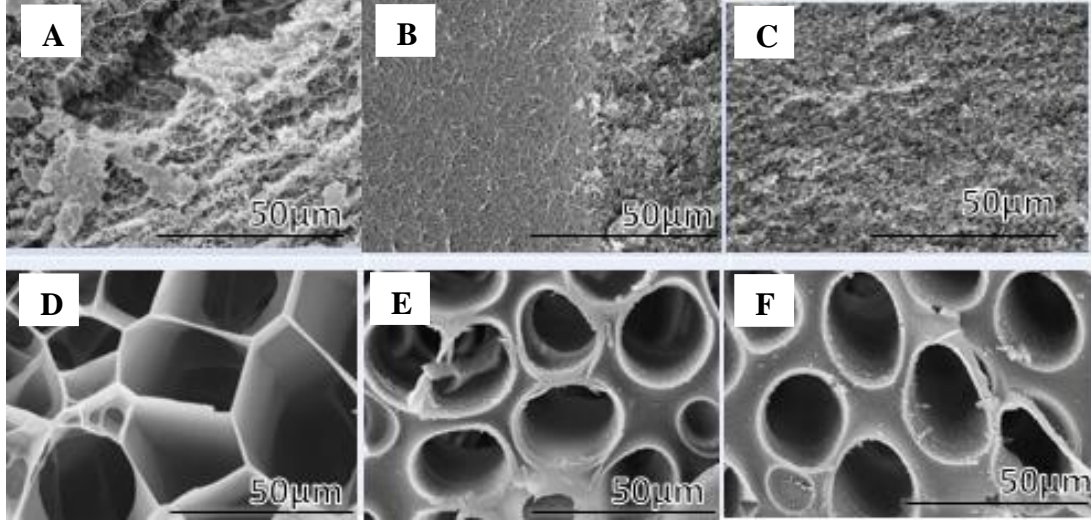


Figure 9. SEM images from samples prepared by drip method A)  $Q_D$ , B)  $Q_D X_{0.35}$  C)  $Q_D X_{0.75}$  D)  $Q_D M$ , E)  $Q_D X_{0.35} M$  F)  $Q_D X_{0.75} M$ .

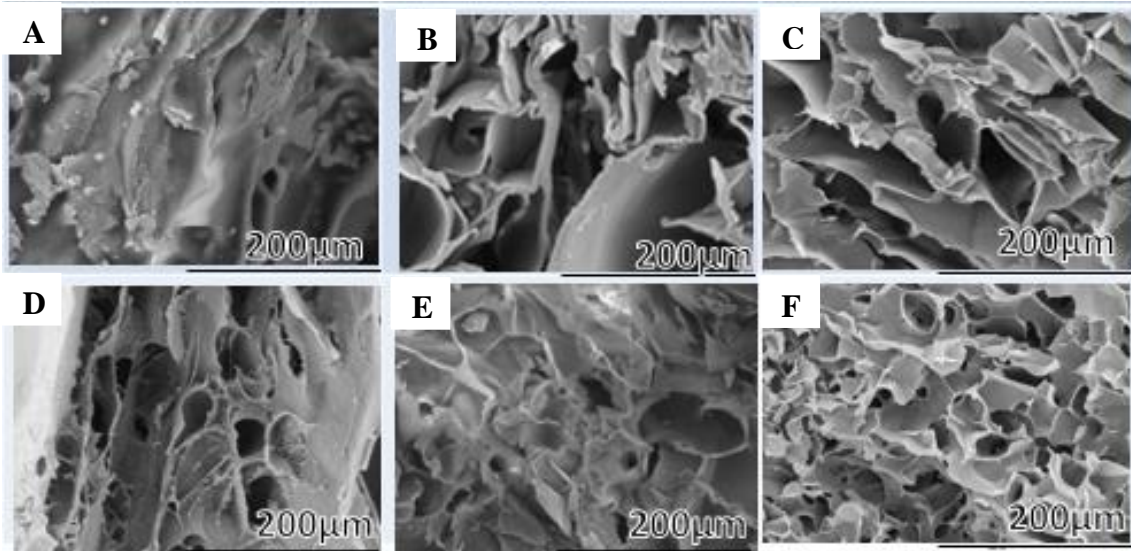


Figure 10. SEM images from samples prepared by solvent evaporated method. A)  $Q_{SE}$ , B)  $Q_{SE} X_{0.35}$  C)  $Q_{SE} X_{0.75}$  D)  $Q_{SE} M$ , E)  $Q_{SE} X_{0.35} M$  and F)  $Q_{SE} X_{0.75} M$ .

Similar morphology was observed by Zhang et al. [15] where the study reveals that the incorporation of magnetic nanoparticles hydrogel networks preserve the porous



morphology nevertheless is possible to observe differences in the shape of the porous and larger pore size. [15] With ordered structures, the concentric multi-layers in CS hydrogels are similar to the wood rings. [7] In addition to the incorporation of magnetite into the polymer matrix, the morphology is being affected by the crosslinker, when CS is chemically crosslinked to prepare hydrogel, the degree of crosslinking can affect the bulk and surface morphology of freeze-dried hydrogels. In the case of the hydrogel of CS prepared by chemically crosslinking with glutaraldehyde, the concentration of glutaraldehyde governs the size and distribution of pores. An increase in the concentration of glutaraldehyde causes the growth of pore size and decreases their distribution by restricting the free movement of the polymer chains. [24, 81, 82]

## 6.2 X-Ray diffraction (XRD) analysis

The powder XRD patterns of samples prepared by the drip method ( $Q_D M$ ,  $Q_D X_{0.35} M$  and  $Q_D X_{0.75} M$ ) and the solvent evaporated method ( $Q_{SE} M$ ,  $Q_{SE} X_{0.35} M$ ,  $Q_{SE} X_{0.75} M$ ) are shown in Figures 12 and 13, respectively. Distinctly, the pattern of the samples can be nearly regarded as a joint combination of the patterns of magnetite and CS. The distinct diffraction peaks at  $2\theta = 30.22^\circ$ ,  $35.62^\circ$ ,  $43.22^\circ$ ,  $53.61^\circ$ ,  $57.28^\circ$ , and  $62.87^\circ$  were assigned to the (220), (311), (222), (400), (422), (511), and (440) planes of  $Fe_3O_4$ . This pattern indicates that  $Fe_3O_4$  magnetic nanoparticles on CS were successfully loaded. The same results have been reported by other researchers. [85] The measurements showed poor crystallinity form for CS. This was indicated by the presence of two broad peaks at  $2\theta = 10.54$  and  $19.98^\circ$ , in agreement with the characteristic diffractogram of the original CS. [32] For all the samples, the crystallinity decreases with the increase of the concentration of glutaraldehyde in the solid gel formed. The XRD patterns of CS appear lower intensity and broader peaks, which indicates greater amorphousness. These peaks may be attributed to that the  $Fe_3O_4$  were embedded in the composite matrix. [71] The pattern shows a more significant reduction in crystallinity for samples prepared by the evaporated solvent method, which suggests that the samples prepared by this method present a higher degree of crosslinking.

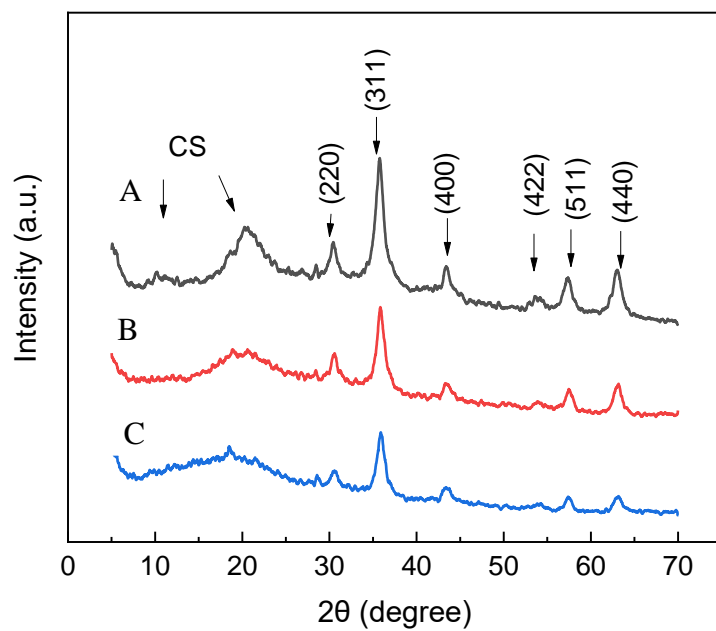


Figure 12. XRD patterns of cross-linked samples A)  $Q_D M$ , B)  $Q_D X_{0.35} M$ , and C)  $Q_D X_{0.75} M$ .

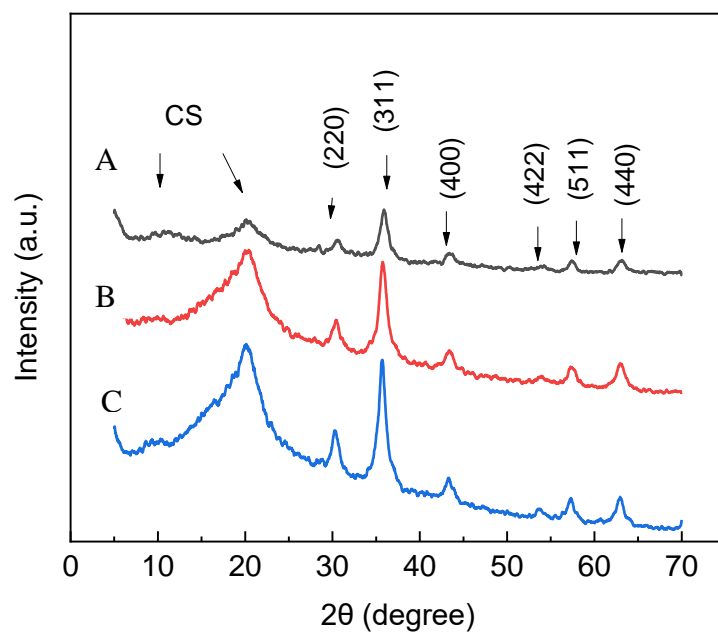


Figure 13. XRD patterns from magnetite hydrogels A)  $Q_{SE} M$ , B)  $Q_{SE} X_{0.35} M$ , and C)  $Q_{SE} X_{0.75} M$ .

With the increase in the concentration of GLA the crystallinity of the samples is affected, the increase of GLA concentration indicates a reduction in its crystallinity. This result is in accordance with Koyama et al., who showed a marked decrease in crystallinity by crosslinking with glutaraldehyde in CS membranes. [37] This can be understood once glutaraldehyde chains were attached and inserted to CS in a previously arranged CS chain configuration, already immobilized in the form of a membrane. This would induce the chemical modification to produce less organized structures than probably the ones that would be gotten if crosslinking was done in homogeneous conditions (in CS solution). [84] The crosslinking of CS with glutaraldehyde induced the attenuation of the peak that depends precisely on the water quantity (0 2 0). This is evidence that the dialdehyde is altering the species that were responsible for water bonding. The crosslinking also induced an increase in the halo of  $21.4^\circ$ , which is due to (2 0 2) reflections, showing that other arrangements were provided after introduction of aldehydic chains. [86]

### 6.3 Swelling

The swelling from the samples was measured by using the data from the TGA of the hydrated samples. Before the test, the sample was placed in distilled water for 24 hours; then, the content of water was possible to obtain in the first transition stage from the thermal analysis. Table 4 indicates the swelling ratio of the samples.

*Table 4. The swelling ratio for different samples prepared in this work.*

<i>Sample</i>	<i>Swelling (%)</i>
$Q_D$	1438
$Q_D X_{0.35}$	1093
$Q_D X_{0.75}$	1062
$Q_D M$	1090
$Q_D X_{0.35} M$	852
$Q_D X_{0.75} M$	831
$Q_{SE}$	789
$Q_{SE} X_{0.35}$	563
$Q_{SE} X_{0.75}$	759
$Q_{SE} M$	505.
$Q_{SE} X_{0.35} M$	560
$Q_{SE} X_{0.75} M$	609

The samples prepared by the drip method present more content of water than the samples prepared by the solvent evaporated method, this change may be attributed to the higher crosslinked of the solvent evaporated samples. The increase in the amount of GLA implies a decrease in the swelling ratio of the samples prepared by the drip method. The incorporation of magnetite particles in the polymer matrix of the samples affects the swelling ratio by decreasing it. Crosslinking resulted in the gel structure becoming more compact which did not allow significant swelling and shrinking. [83] The addition of magnetite nanoparticles formed a tight and dense structure, hindering the diffusion of water through the hydrogel and leading to a decrease in water absorbency. [7]

#### **6.4 Thermal stability**

The TGA provides information about the composition of the sample, decomposition reaction, and moisture content. TGA results for CS, and the cross-linked and magnetic modified polymers prepared by the drip method are shown in Figure 14 and in Table 5 where the table of results indicate the temperature of the start and the ends of the main stages in the thermal analysis of the samples, the weight loss, the degradation temperature and the total weight loss of the hydrogels.

The thermal analysis of the freeze-dried beads indicates three main stages. An initial weight loss of around 6% for the samples  $Q_D$ ,  $Q_DX_{0.35}$ ,  $Q_DX_{0.75}$  and 4% for the samples  $Q_DM$ ,  $QDX_{0.35}M$ ,  $QDX_{0.75}M$  below 120 °C is attributed to the loss of water; this behavior confirms that the samples are hygroscopic, and the tendency indicates that the samples with magnetite present less content of moisture. The second stage is characterized by a decomposition event for the CS hydrogels between 200 and 400 °C. Non crosslinked samples ( $Q_D$  and  $Q_DM$ ) decomposes near 215 °C while the crosslinked polymers ( $Q_DX_{0.35}$ ,  $Q_DX_{0.75}$ ,  $QDX_{0.35}M$ ,  $QDX_{0.75}M$ ) decompose at lower temperatures (< 215 °C), in agreement with the literature. [79, 80]

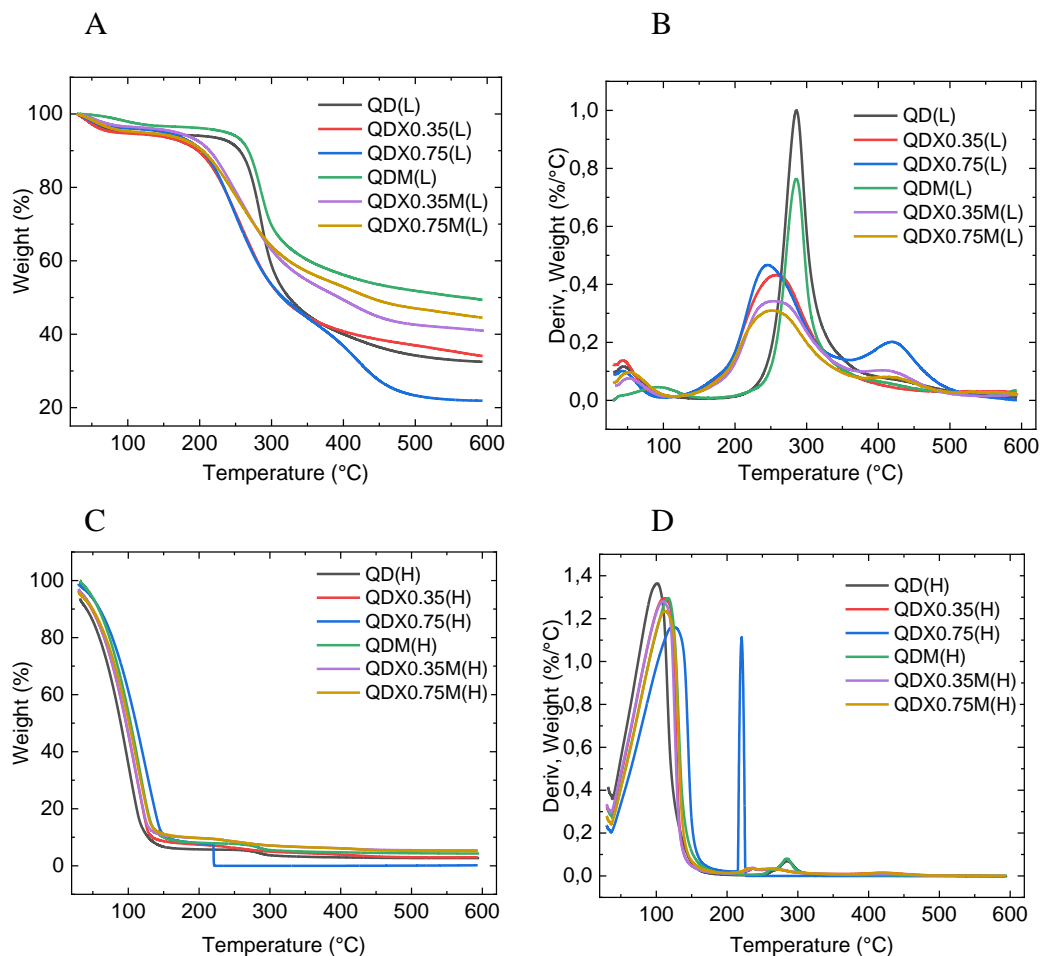


Figure 14. Thermal analysis for hydrated samples of hydrogels prepared by drip method. A) TGA for freeze dried samples B) DTG for freeze dried samples C) TGA for hydrated samples D) DTG for hydrated samples.

Beppu et al. have reported TGA results for CS crosslinked with glutaraldehyde and a transition were observed ( $<300\text{ }^{\circ}\text{C}$ ), which is significantly broadened relative to pristine CS. The reduced temperature onset observed for the crosslinked polymers may be attributed to the effect of crosslinking because it is anticipated to reduce the thermal stability due to attenuation of the intermolecular H-bonding between adjacent CS polymer units. [79,81] The event at  $\sim 460\text{ }^{\circ}\text{C}$  occurs within the thermal decomposition range anticipated for the glutaraldehyde crosslinker domains of the polymer materials.

Table 5. TGA results of freeze-dried samples (L) prepared by drip method.

Sample	Stage	W. Loss (%)	Onset T (°C)	Endset T (°C)	Degr T, (°C)	Total W Loss (%)
$Q_D$ (L)	1st stage	5.66	30	90.12	45.59	67.54
	2nd stage	48.85	213	348	286.11	
$Q_DX_{0.35}$ (L)	1st stage	5.41	30	90.12	42.96	65.985
	2nd stage	53.67	146	400	259.39	
$Q_DX_{0.75}$ (L)	1st stage	7.89	30	92.18	43.73	78.1
	2nd stage	53.76	187	360	244.6	
	3rd stage	31.52	365	500	418.75	
$Q_DM$ (L)	1st stage	3.5	30	96	92.97	50.74
	2nd stage	40.05	223	433	286.19	
$Q_DX_{0.35}M$ (L)	1st stage	3.69	30	103.19	51.66	59.48
	2nd stage	41.44	135	355	255.75	
	3rd stage	12.81	355	522	408.06	
$Q_DX_{0.75}M$ (L)	1st stage	4.8	30	107.13	52.16	55.54
	2nd stage	39.41	129,38	366.6	250.33	
	3rd stage	9.87	382.7	525.92	420.58	

Table 6. TGA results of freeze-dried samples prepared by the solvent evaporated method

Sample	Stage	W. Loss (%)	Onset T (°C)	Endset T (°C)	Degr T, (°C)	Total W Loss (%)
$Q_{SE}$ (L)	1st stage	4.98	30.00	117.99	46.43	63.58
	2nd stage	49.93	204.24	412.03	287.18	
$Q_{SE}X_{0.35}$ (L)	1st stage	5.60	30.00	128.48	70.60	59.59
	2nd stage	42.63	190.00	356.98	277.20	
$Q_{SE}X_{0.75}$ (L)	1st stage	5.83	30.00	127.55	60.58	65.04
	2nd stage	43.87	176.58	372.39	271.63	
	3rd stage	11.92	376.54	495.05	429.32	
$Q_{SE}M$ (L)	1st stage	5.95	30.00	121.10	47.73	56.18
	2nd stage	40.06	196.03	378.89	282.82	
$Q_{SE}X_{0.35}M$ (L)	1st stage	5.45	30.00	129.602	67.50	52.04
	2nd stage	40.03	159.42	404.80	274.11	
$Q_{SE}X_{0.75}M$ (L)	1st stage	6	30	145.43	76.78	53.69
	2nd stage	40.71	165.42	401	271.63	

The TGA results for solvent evaporated methods shown in Figure 15 and Table 6 indicate weight loss in three stages: around at around 90 °C due to the release of typical hydrogen-bonded water, and a second weight loss starting at 200 °C and ending at 300 °C, corresponds to the thermal and oxidative decomposition of CS and vaporization and the elimination of volatile products. Table 6 indicates that the crosslinked samples prepared by the solvent evaporated method slightly increase the thermal stability of the hydrogels. This difference in the thermal stability of samples prepared by the drip method and solvent evaporated method can be related to the degree of crosslinking. Since the glutaraldehyde concentration was diluted in water for the drip method, it implies that the crosslinking degree was low too. A possible explanation for the decrease of thermal stability at a low degree of crosslinking would be the formation of intra-crosslinking reactions between polysaccharides chains, which by its turn, interferes with previously existing attractive hydrogen bonds, in those regions where crosslinking occurred. As a consequence, the crosslinked polymer's structure weakened, reducing its thermal stability. [89]

On the other hand, the crosslinking samples prepared by the solvent evaporated method indicate a higher degree of crosslinking. The addition of magnetite implies high thermal stability for all the samples which correlate with the observed in the literature. [11, 83, 84] The proposed explanation by some authors is related to the restrictions in polymer chain mobility and to the reduction of diffusivity of attacking agents within the polymer matrix, both due to the polymer-filler interactions. Thus, the nanoparticles may act as a heating barrier. In the present case, the polymer nanoparticle interaction could be a type of adhesive force.

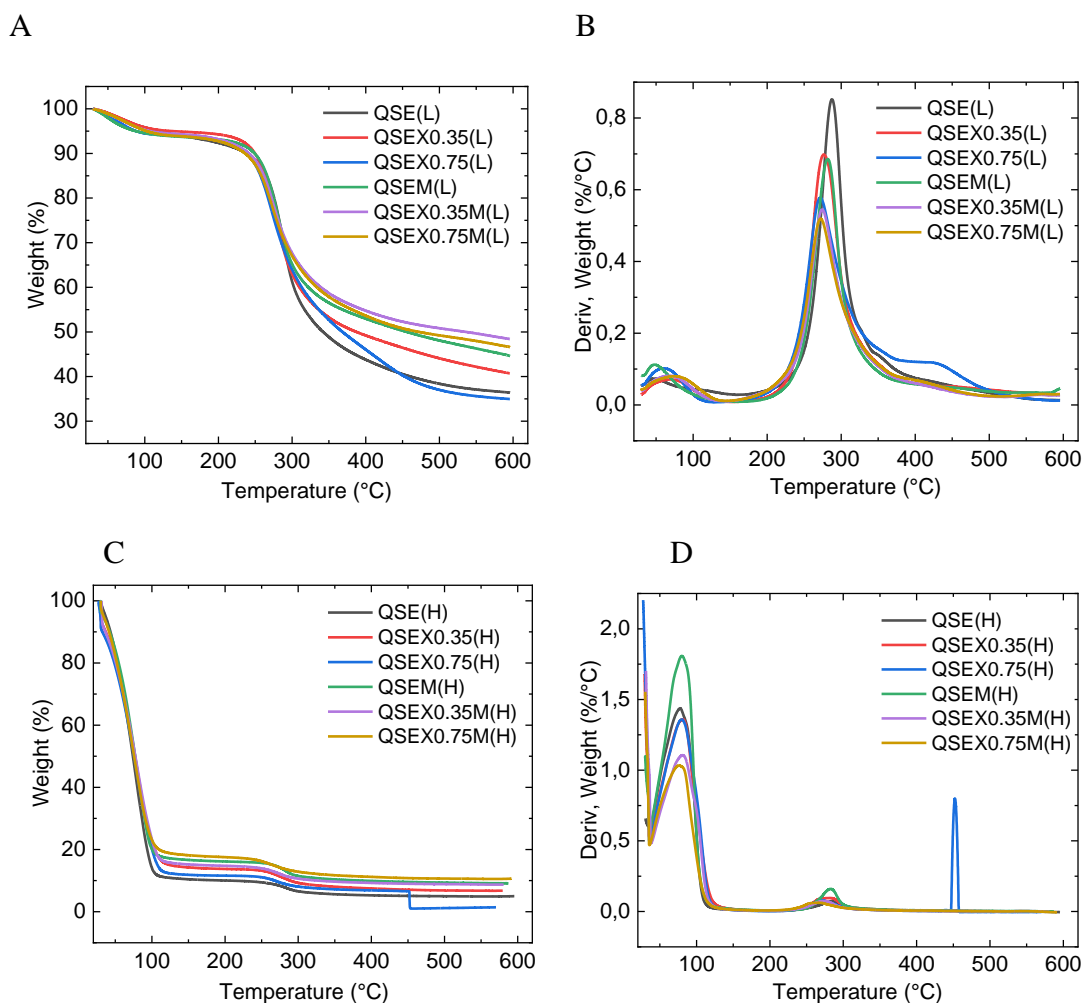


Figure 15. Thermal analysis for freeze-dried (L) and hydrated (H) samples of hydrogels prepared by solvent evaporated method. A) TGA for freeze-dried samples B) DTG for freeze-dried samples C) TGA for hydrated samples D) DTG for hydrated samples.

From the total weight loss is possible to estimate the magnetite content of the samples, where  $Q_D M$ ,  $Q_D X_{0.35} M$ ,  $Q_D X_{0.75} M$  16.8%, 6.5%, 22% respectively, and for the solvent evaporated samples  $Q_{SE} M$ ,  $Q_{SE} X_{0.35} M$  and  $Q_{SE} X_{0.75} M$  the estimated content is 7.4%, 7.55% and 11.35% , respectively.

The kinetic parameters for freeze-dried samples were calculated by using Friedman Method. The activation energy and the decomposition reaction order are shown in Table 7, the complementary parameters as correlation coefficient (r1 and r2) and the



pre exponential factor ( $A$ ) are shown in the Table 5A in the annex. The results indicate higher values of activation energy for samples prepared by solvent evaporated method, a decrease in the activation energy with the increase in GLA, and higher values of activation energy with the addition of magnetite nanoparticles, which is in agreement with the data obtained from the TGA curves; by this means the activation energy ( $Ea$ ) is the energy required for the onset of degradation, therefore the higher the activation energy, the higher the thermal stability of a polymer and vice versa.

*Table 7. Kinetic parameters for freeze-dried CS-based hydrogels samples prepared by drip method at a heating rate 10 °C/min.*

<i>Samples</i>	<i>Ea (kJ/mol)</i>	<i>n</i>
$Q_D$	33033	3.19
$Q_D X_{0.35}$	10362	3.12
$Q_D X_{0.75}$	11971	2.76
$Q_D M$	37668	3.59
$Q_D X_{0.35} M$	12004	2.98
$Q_D X_{0.75} M$	1159	2.63
$Q_{SE}$	32162	4.70
$Q_{SE} X_{0.35}$	24624	5.89
$Q_{SE} X_{0.75}$	18856	6.30
$Q_{SE} M$	29389	4.32
$Q_{SE} X_{0.35} M$	23635	5.90
$Q_{SE} X_{0.75} M$	20459	5.28

The increase in activation energy with the decrease in the GLA concentration indicates that the rate of cross-linking can be limited by the mobility of longer polymer chains. [92] By this means, the two polar groups, hydroxyl and amine present in the structure of the CS macromolecule, allow the bonding with water molecules of the surrounding. Several studies of the structure of CS performed by infrared investigation determine the strength of interaction of water with the polar groups, where it was found that the interaction water with hydroxyl groups is stronger than with amine groups. [89] Since amine groups are transformed into imines during the cross-linking reaction, it can be deduced for the crosslinked-CS sample that the available amine groups for the interaction with water will be smaller. Thus, some water molecules that would be bound to amine groups will now be bound to hydroxyl groups. [89]

## 7. Conclusion

In this work was possible to synthesize magnetic CS-based hydrogels crosslinked with glutaraldehyde by drip and solvent evaporated method. Scanning Electron Microscopy confirms the porosity of the samples. The morphology was affected by the method of preparation, the samples prepared by solvent evaporated method present large, irregular and elongated pores, in contrast with the porous of the samples prepared by drip method which are small and with well defined shape. The crosslinked samples show a tendency to decrease its pore size diameter with an increase in the concentration of glutaraldehyde. Moreover, the incorporation of magnetite particles influences the pore size diameter by increasing it.

X-rays diffraction provides broad peaks at  $2\theta = 30.22^\circ$ ,  $35.62^\circ$ ,  $43.22^\circ$ ,  $53.61^\circ$ ,  $57.28^\circ$ , and  $62.87^\circ$  which are consistent with the peaks of magnetite, therefore, the presence of magnetite particles is confirmed and the reduction in cristallinity indicate the crosslinked of the samples. The swelling test indicate that samples prepared by drip method swell more than the samples prepared by solvent evaporated method; the increase in concentration of GLA and the incorporation of magnetite nanoparticles implies less swell of the samples. Moreover, the characterization indicate that the samples prepared by solvent evaporated method are higher crosslinked than the ones prepared by drip method. The thermal analysis of the samples indicates a reduction in thermal stability for crosslinked samples prepared by drip method and a slightly increase for samples prepared by solvent evaporated method. Due to its great capacity of swelling, its thermal stability and the prescence of magnetite into the polymer matrix, the hydrogels may be suitable for the application of wastewater treatment.

## 8. Annex 1

### 8.1 SEM

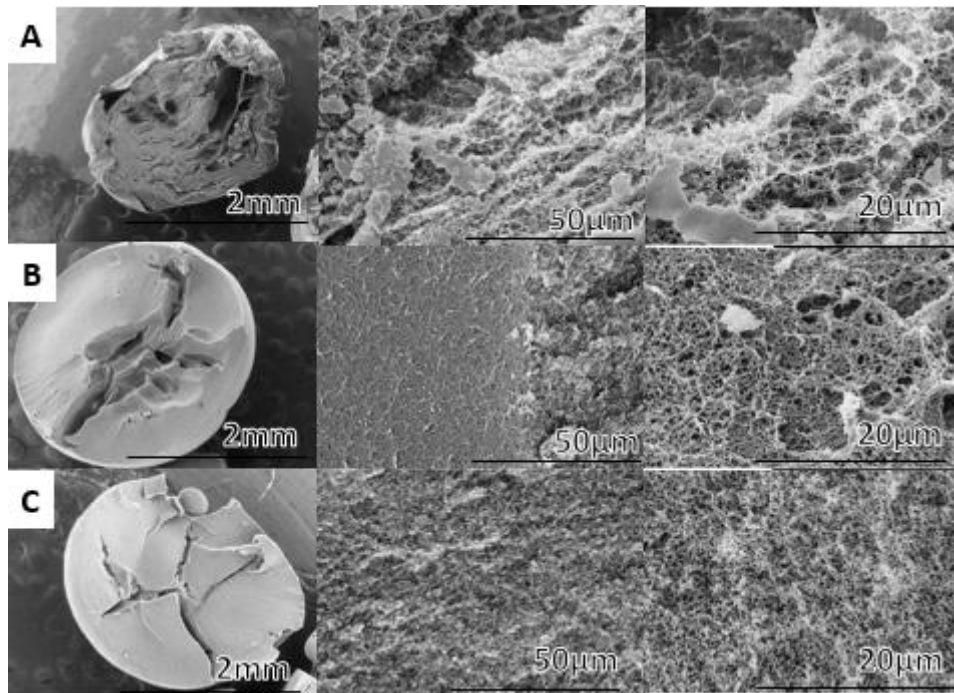


Figure 1A. SEM images from samples prepared by drip method A)  $Q_D$ , B)  $Q_D X_{0.35}$ , C)  $Q_D X_{0.75}$  at different scales

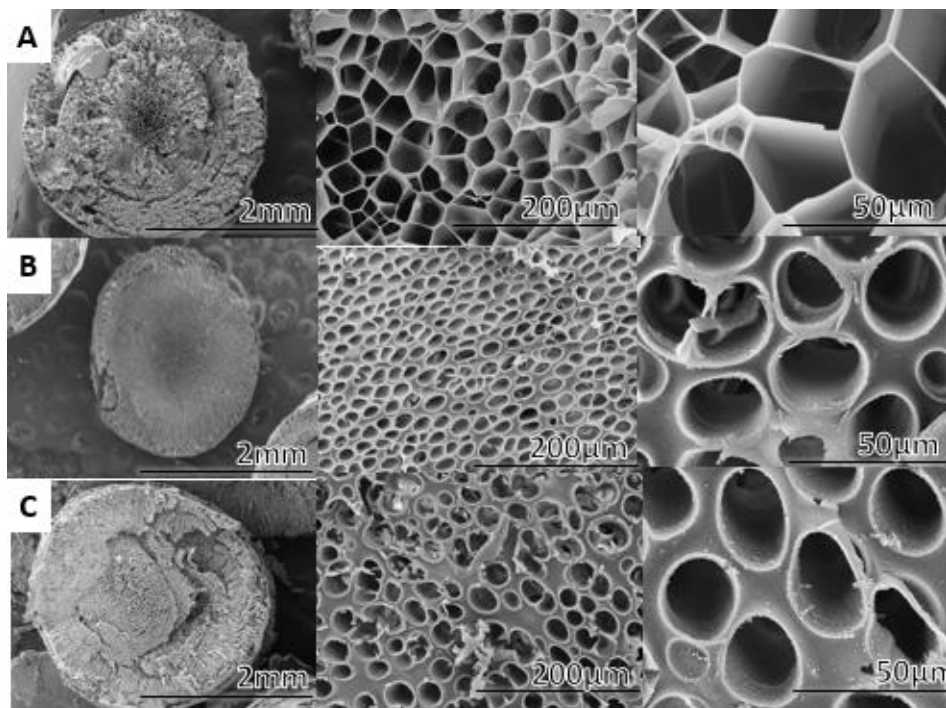


Figure 2A. SEM images from samples prepared by drip method A)  $Q_D M$ , B)  $Q_D X_{0.35} M$ , C)  $Q_D X_{0.75} M$  at different scales.

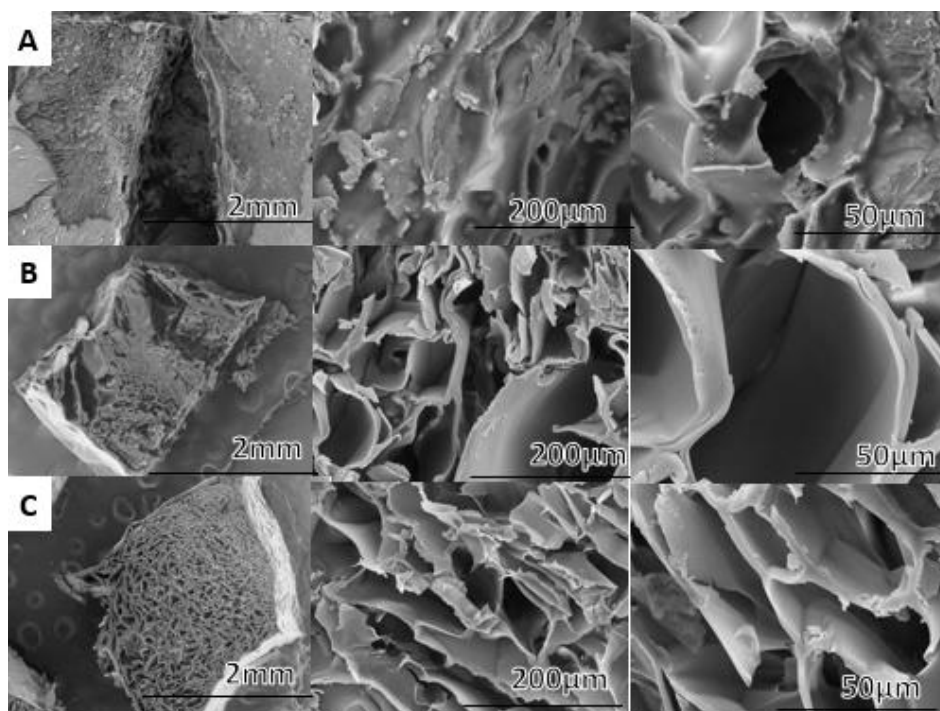


Figure 3A. SEM images form samples prepared by solvent evaporated method A)  $Q_{SE}$ , B)  $Q_{SE}X_{0.35}$ , C)  $Q_{SE}X_{0.75}$  at different scales.

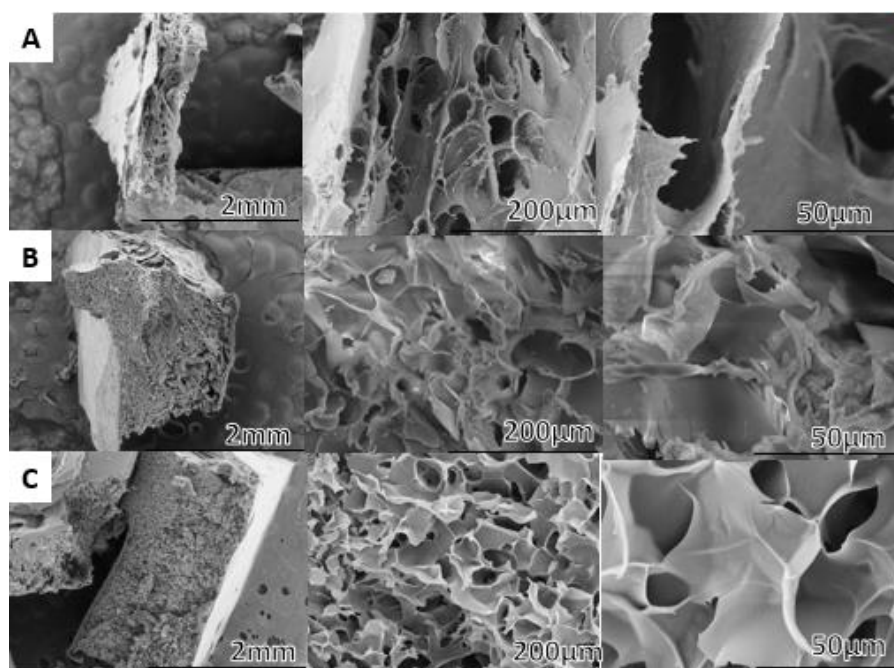


Figure 4A. SEM images form samples prepared by solvent evaporated method A)  $Q_{SE}M$ , B)  $Q_{SE}X_{0.35}M$ , C)  $Q_{SE}X_{0.75}M$  at different scales.

## 8.2 TGA

Table A1. TGA results of freeze dried samples prepared by drip method.

<i>Sample</i>	<i>Stage</i>	<i>W. Loss (%)</i>	<i>Onset T (°C)</i>	<i>Endset T (°C)</i>	<i>Degr T.(°C)</i>	<i>Total W Loss (%)</i>
$Q_D(L)$	1st stage	5.66	30	90.12	45.59	67.54
	2nd stage	48.85	213	348	286.11	
$Q_DX_{0.35}(L)$	1st stage	5.41	30	90.12	42.96	65.98
	2nd stage	53.67	146	400	259.39	
$Q_DX_{0.75}(L)$	1st stage	7.89	30	92.18	43.73	78.10
	2nd stage	53.76	187	360	244.6	
	3rd stage	31.52	365	500	418.75	
$Q_DM(L)$	1st stage	3.50	30	96	92.97	50.74
	2nd stage	40.05	223	433	286.19	
$Q_DX_{0.35}M(L)$	1st stage	3.69	30	103.19	51.66	59.48
	2nd stage	41.44	135	355	255.75	
	3rd stage	12.81	355	522	408.06	
$Q_DX_{0.75}M(L)$	1st stage	4.80	30	107.13	52.16	55.54
	2nd stage	39.41	129.38	366.60	250.33	
	3rd stage	9.87	382.7	525.92	420.58	

Table A2. TGA results of freeze dried samples prepared by solvent evaporated method.

<i>Sample</i>	<i>Stage</i>	<i>W. Loss (%)</i>	<i>Onset T (°C)</i>	<i>Endset T (°C)</i>	<i>Degr T.(°C)</i>	<i>Total W Loss (%)</i>
$Q_{SE}(L)$	1st stage	4.98	30	117.99	46.43	63.58
	2nd stage	49.93	204.24	412.03	287.18	
$Q_{SE}X_{0.35}(L)$	1st stage	5.60	30	128.48	70.60	59.59
	2nd stage	42.63	190	356.98	277.20	
$Q_{SE}X_{0.75}(L)$	1st stage	5.83	30	127.55	60.58	65.04
	2nd stage	43.87	176.58	372.39	271.63	
	3rd stage	11.92	376.54	495.05	429.32	
$Q_{SE}M(L)$	1st stage	5.95	30	121.1	47.73	56.18
	2nd stage	40.06	196.03	378.89	282.82	
$Q_{SE}X_{0.35}M(L)$	1st stage	5.45	30	129.60	67.50	52.04
	2nd stage	40.03	159.42	404.80	274.11	
$Q_{SE}X_{0.75}M(L)$	1st stage	6	30	145.43	76.78	53.69
	2nd stage	40.71	165.42	401	271.63	

Table A3. TGA results of hydrated samples prepared by drip method.

Sample	Stage	W. Loss (%)	Onset T (°C)	Endset T (°C)	Degr T.(°C)	Total W Loss (%)
$Q_D(H)$	1st stage	93.50	30	159.18	101.08	97.13
	2nd stage	2.66	250.59	338.04	264.55	
$Q_DX_{0.35}(H)$	1st stage	91.62	30	161.45	114.08	96.89
	2nd stage	2.86	225	249	237.20	
	3rd stage	1.43	250	292	256.45	
$Q_DX_{0.75}(H)$	1st stage	91.40	30	171.78	115.38	99.81
	2nd stage	7.28	220	222.37	219.22	
$Q_DM(H)$	1st stage	91.62	30	178.05	116.68	95.78
	2nd stage	2.82	234.94	321.06	261.71	
$Q_DX_{0.35}M(H)$	1st stage	89.49	30	164.47	112.78	94.40
	2nd stage	3.52	193.31	367	235.45	
$Q_DX_{0.75}M(H)$	1st stage	89.27	30	166.79	111.48	94.62
	2nd stage	90.37	176.37	371.53	230.22	

Table A4. TGA results of hydrated samples prepared by solvent evaporated method.

Sample	Stage	W. Loss (%)	Onset T (°C)	Endset T (°C)	Degr T.(°C)	Total W Loss (%)
$Q_{SE}(H)$	1st stage	88.76	30	111.47	77.42	95.02
	2nd stage	4.62	213.33	342.94	284.48	
$Q_{SE}X_{0.35}(H)$	1st stage	84.92	30	157.09	79.90	93.23
	2nd stage	5.85	224.31	349.29	276.48	
$Q_{SE}X_{0.75}(H)$	1st stage	88.36	30	153.45	79.91	98.49
	2nd stage	4.62	234.18	350.44	269.87	
	3rd stage	5.60	451.41	453.36	451.58	
$Q_{SE}M(H)$	1st stage	83.49	30	146.09	81.2	90.85
	2nd stage	5.57	242.85	349.28	282.87	
$Q_{SE}X_{0.35}M(H)$	1st stage	84.87	30	145.32	82.38	91.26
	2nd stage	5.30	219.73	350.44	273.28	
$Q_{SE}X_{0.75}M(H)$	1st stage	85.91	30	147.56	76.25	89.37
	2nd stage	5.99	207.54	346.41	260.5	

Table 5A. Kinetic parameters of hydrogels samples at a heating rate 10 °C/min.

<i>Samples</i>	<i>Ea (KJ/mol)</i>	<i>n</i>	<i>A</i>	<i>r1</i>	<i>r2</i>
$Q_D$	33033	3.19	0.008	0.996	0.981
$Q_D X_{0.35}$	10362	3.13	3.36	0.990	0.964
$Q_D X_{0.75}$	11971	2.76	0.96	0.994	0.988
$Q_D M$	37668	3.59	0.00058	0.996	0.972
$Q_D X_{0.35} M$	12004	2.98	2.24	0.996	0.990
$Q_D X_{0.75} M$	9159	2.63	3.37	0.986	0.988
$Q_{SE}$	32162	4.70	0.01	0.998	0.979
$Q_{SE} X_{0.35}$	24624	5.89	9.95	0.990	0.935
$Q_{SE} X_{0.75}$	18856	6.30	0.49	0.984	0.947
$Q_{SE} M$	29389	4.32	0.022	0.998	0.967
$Q_{SE} X_{0.35} M$	23635	5.90	2.52	0.991	0.985
$Q_{SE} X_{0.75} M$	20459	5.28	7.17	0.990	0.986



## 9. REFERENCES

- [1] S. Rafieian, H. Mirzadeh, H. Mahdavi, and M. E. Masoumi, "A review on nanocomposite hydrogels and their biomedical applications," *IEEE J. Sel. Top. Quantum Electron.*, vol. 26, no. 1, pp. 154–174, 2019, doi: 10.1515/secm-2017-0161.
- [2] M. G. Pineda *et al.*, "Chitosan-coated magnetic nanoparticles prepared in one-step by precipitation in a high- Aqueous phase content reverse microemulsion," *Molecules*, vol. 19, no. 7, pp. 9273–9287, 2014, doi: 10.3390/molecules19079273.
- [3] O. M, L. W, and K. N, *Treatment of Radioactive Wastes*. 2019.
- [4] M. Vakili *et al.*, "Application of chitosan and its derivatives as adsorbents for dye removal from water and wastewater: A review," *Carbohydr. Polym.*, vol. 113, pp. 115–130, 2014, doi: 10.1016/j.carbpol.2014.07.007.
- [5] L. Racine, I. Texier, and R. Auzély-Velty, "Chitosan-based hydrogels: recent design concepts to tailor properties and functions," *Polym. Int.*, vol. 66, no. 7, pp. 981–998, 2017, doi: 10.1002/pi.5331.
- [6] A. H. Shalla, M. A. Bhat, and Z. Yaseen, "Hydrogels for removal of recalcitrant organic dyes: A conceptual overview," *J. Environ. Chem. Eng.*, vol. 6, no. 5, pp. 5938–5949, 2018, doi: 10.1016/j.jece.2018.08.063.
- [7] J. Liao and H. Huang, "Review on Magnetic Natural Polymer Constructed Hydrogels as Vehicles for Drug Delivery," *Biomacromolecules*, vol. 21, no. 7, pp. 2574–2594, 2020, doi: 10.1021/acs.biomac.0c00566.
- [8] J. Nilsen-Nygaard, S. P. Strand, K. M. Vårum, K. I. Draget, and C. T. Nordgård, "Chitosan: Gels and interfacial properties," *Polymers (Basel)*, vol. 7, no. 3, pp. 552–579, 2015, doi: 10.3390/polym7030552.
- [9] K. Ravishankar and R. Dhamodharan, "Advances in chitosan-based hydrogels: Evolution from covalently crosslinked systems to ionotropically crosslinked superabsorbents," *React. Funct. Polym.*, vol. 149, p. 104517, 2020, doi: 10.1016/j.reactfunctpolym.2020.104517.

- [10] P. Mohammadzadeh Pakdel and S. J. Peighambaroust, "Review on recent progress in chitosan-based hydrogels for wastewater treatment application," *Carbohydr. Polym.*, vol. 201, pp. 264–279, 2018, doi: 10.1016/j.carbpol.2018.08.070.
- [11] V. K. Thakur and M. R. Kessler, "Self-healing polymer nanocomposite materials: A review," *Polymer (Guildf)*, vol. 69, pp. 369–383, 2015, doi: 10.1016/j.polymer.2015.04.086.
- [12] M. Abbasi, "Synthesis and characterization of magnetic nanocomposite of chitosan/SiO<sub>2</sub>/carbon nanotubes and its application for dyes removal," *J. Clean. Prod.*, vol. 145, pp. 105–113, 2017, doi: 10.1016/j.jclepro.2017.01.046.
- [13] T. Józwiak, U. Filipkowska, P. Szymczyk, and M. Zyśk, "Effect of the form and deacetylation degree of chitosan sorbents on sorption effectiveness of Reactive Black 5 from aqueous solutions," *Int. J. Biol. Macromol.*, vol. 95, pp. 1169–1178, 2017, doi: 10.1016/j.ijbiomac.2016.11.007.
- [14] J. Li *et al.*, "Brilliant red X-3B uptake by a novel polycyclodextrin-modified magnetic cationic hydrogel: Performance, kinetics and mechanism," *J. Environ. Sci. (China)*, vol. 89, pp. 264–276, 2020, doi: 10.1016/j.jes.2019.09.008.
- [15] C. Zhang *et al.*, "Facile preparation of polyacrylamide / chitosan / Fe<sub>3</sub>O<sub>4</sub> composite hydrogels for effective removal of methylene blue from aqueous solution," *Carbohydr. Polym.*, vol. 234, no. January, p. 115882, 2020, doi: 10.1016/j.carbpol.2020.115882.
- [16] H. V. Tran, L. D. Tran, and T. N. Nguyen, "Preparation of chitosan/magnetite composite beads and their application for removal of Pb(II) and Ni(II) from aqueous solution," *Mater. Sci. Eng. C*, vol. 30, no. 2, pp. 304–310, 2010, doi: 10.1016/j.msec.2009.11.008.
- [17] M. V. Dinu, I. A. Dinu, M. M. Lazar, and E. S. Dragan, "Chitosan-based ion-imprinted cryo-composites with excellent selectivity for copper ions," *Carbohydr. Polym.*, vol. 186, no. January, pp. 140–149, 2018, doi: 10.1016/j.carbpol.2018.01.033.
- [18] M. Khan and I. M. C. Lo, "A holistic review of hydrogel applications in the adsorptive removal of aqueous pollutants: Recent progress, challenges, and

- perspectives,” *Water Res.*, vol. 106, pp. 259–271, 2016, doi: 10.1016/j.watres.2016.10.008.
- [19] E. Y. Danish, E. M. Bakhsh, and K. Akhtar, “Design of chitosan nanocomposite hydrogel for sensitive detection and removal of organic pollutants,” *Int. J. Biol. Macromol.*, vol. 159, pp. 276–286, 2020, doi: 10.1016/j.ijbiomac.2020.05.036.
- [20] I. Aranaz, M. C. Gutiérrez, M. L. Ferrer, and F. Del Monte, “Preparation of chitosan nanocomposites with a macroporous structure by unidirectional freezing and subsequent freeze-drying,” *Mar. Drugs*, vol. 12, no. 11, pp. 5619–5642, 2014, doi: 10.3390/md12115619.
- [21] S. Maji, T. Agarwal, J. Das, and T. K. Maiti, *Development of gelatin/carboxymethyl chitosan/nano-hydroxyapatite composite 3D macroporous scaffold for bone tissue engineering applications*. Elsevier Ltd., 2018.
- [22] A. M. Salgado-Delgado *et al.*, “Morphological and thermal characterization of a high porous composite of biomaterial PHEMA-chitosan-ceramic (Hydroxyapatite),” *Rev. Mex. Ing. Quim.*, vol. 15, no. 2, pp. 625–632, 2016.
- [23] L. Das, P. Das, A. Bhowal, and C. Bhattacharjee, “Synthesis of hybrid hydrogel nano-polymer composite using Graphene oxide, Chitosan and PVA and its application in waste water treatment,” *Environ. Technol. Innov.*, vol. 18, p. 100664, 2020, doi: 10.1016/j.eti.2020.100664.
- [24] T. Kamal, Y. Anwar, S. B. Khan, M. T. S. Chani, and A. M. Asiri, “Dye adsorption and bactericidal properties of TiO<sub>2</sub>/chitosan coating layer,” *Carbohydr. Polym.*, vol. 148, pp. 153–160, 2016, doi: 10.1016/j.carbpol.2016.04.042.
- [25] G. Crini, G. Torri, E. Lichtfouse, G. Z. Kyzas, L. D. Wilson, and N. Morin-Crini, *Cross-Linked Chitosan-Based Hydrogels for Dye Removal*. 2019.
- [26] M. S. Rahman *et al.*, *Morphological Characterization of Hydrogels*. 2019.
- [27] O. Guise, C. Strom, and N. Preschilla, “STEM-in-SEM method for morphology analysis of polymer systems,” *Polymer (Guildf.)*, vol. 52, no. 5, pp. 1278–1285, 2011, doi: 10.1016/j.polymer.2011.01.030.
- [28] T. Durance and P. Yaghmaee, *Microwave Dehydration of Food and Food*

*Ingredients*, Second Edi., vol. 4. Elsevier B.V., 2011.

- [29] M. V. Risbud, A. A. Hardikar, S. V. Bhat, and R. R. Bhonde, "pH-sensitive freeze-dried chitosan-polyvinyl pyrrolidone hydrogels as controlled release system for antibiotic delivery," *J. Control. Release*, vol. 68, no. 1, pp. 23–30, 2000, doi: 10.1016/S0168-3659(00)00208-X.
- [30] R. Eivazzadeh-Keihan, F. Radinekiyan, A. Maleki, M. Salimi Bani, Z. Hajizadeh, and S. Asgharnasl, "A novel biocompatible core-shell magnetic nanocomposite based on cross-linked chitosan hydrogels for in vitro hyperthermia of cancer therapy," *Int. J. Biol. Macromol.*, vol. 140, pp. 407–414, 2019, doi: 10.1016/j.ijbiomac.2019.08.031.
- [31] B. M. C. Gutiérrez *et al.*, "Poly ( vinyl alcohol ) Scaffolds with Tailored Morphologies for Drug Delivery and Controlled Release \*\*," pp. 3505–3513, 2007, doi: 10.1002/adfm.200700093.
- [32] S. A. Bencherif, T. M. Braschler, and P. Renaud, "Advances in the design of macroporous polymer scaffolds for potential applications in dentistry," pp. 251–261, 2013.
- [33] P. Rai, R. K. Gautam, S. Banerjee, V. Rawat, and M. C. Chattopadhyaya, "Synthesis and characterization of a novel SnFe<sub>2</sub>O<sub>4</sub>@activated carbon magnetic nanocomposite and its effectiveness in the removal of crystal violet from aqueous solution," *J. Environ. Chem. Eng.*, vol. 3, no. 4, pp. 2281–2291, 2015, doi: 10.1016/j.jece.2015.08.017.
- [34] A. Memic *et al.*, "Latest Advances in Cryogel Technology for Biomedical Applications," *Adv. Ther.*, vol. 2, no. 4, p. 1800114, 2019, doi: 10.1002/adtp.201800114.
- [35] M. V. Dinu, A. I. Cocarta, and E. S. Dragan, "Synthesis, characterization and drug release properties of 3D chitosan/clinoptilolite biocomposite cryogels," *Carbohydr. Polym.*, vol. 153, pp. 203–211, 2016, doi: 10.1016/j.carbpol.2016.07.111.
- [36] E. S. Dragan and M. V. Dinu, "Advances in porous chitosan-based composite hydrogels: Synthesis and applications," *React. Funct. Polym.*, vol. 146, no. September 2019, p. 104372, 2020, doi: 10.1016/j.reactfunctpolym.2019.104372.

- [37] E. S. Dragan, D. Humelnicu, and M. V. Dinu, "Development of chitosan-poly(ethyleneimine) based double network cryogels and their application as superadsorbents for phosphate," *Carbohydr. Polym.*, vol. 210, no. November 2018, pp. 17–25, 2019, doi: 10.1016/j.carbpol.2019.01.054.
- [38] C. Ji, N. Annabi, A. Khademhosseini, and F. Dehghani, "Acta Biomaterialia Fabrication of porous chitosan scaffolds for soft tissue engineering using dense gas CO<sub>2</sub>," *Acta Biomater.*, vol. 7, no. 4, pp. 1653–1664, 2011, doi: 10.1016/j.actbio.2010.11.043.
- [39] D. W. Hutmacher, T. B. F. Woodfield, and P. D. Dalton, *Scaffold Design and Fabrication*, Second Edi. Elsevier Inc., 2015.
- [40] G. Kaynak Bayrak, T. T. Demirtaş, and M. Gümüşderelioğlu, "Microwave-induced biomimetic approach for hydroxyapatite coatings of chitosan scaffolds," *Carbohydr. Polym.*, vol. 157, pp. 803–813, 2017, doi: 10.1016/j.carbpol.2016.10.016.
- [41] T. M. Sampath *et al.*, "Influence of a nonionic surfactant on curcumin delivery of nanocellulose reinforced chitosan hydrogel," *Int. J. Biol. Macromol.*, 2018, doi: 10.1016/j.ijbiomac.2018.06.147.
- [42] T. Sen, B. Ozcelik, and M. M. Ozmen, "Tough and hierarchical porous cryogel scaffolds preparation using n-butanol as a non-solvent," *Int. J. Polym. Mater. Polym. Biomater.*, vol. 68, no. 7, pp. 411–416, 2018, doi: 10.1080/00914037.2018.1452225.
- [43] Y. Wang, B. Li, Y. Zhou, Z. Han, Y. Feng, and D. Wei, "A facile concentric-layered magnetic chitosan hydrogel with magnetic field remote stimulated drug release," *J. Control. Release*, vol. 172, no. 1, p. e90, 2013, doi: 10.1016/j.jconrel.2013.08.182.
- [44] F. L. Mi, S. J. Wu, and Y. C. Chen, "Combination of carboxymethyl chitosan-coated magnetic nanoparticles and chitosan-citrate complex gel beads as a novel magnetic adsorbent," *Carbohydr. Polym.*, vol. 131, pp. 255–263, 2015, doi: 10.1016/j.carbpol.2015.06.031.
- [45] E. S. Dragan, M. M. Perju, and M. V. Dinu, "Preparation and characterization of IPN composite hydrogels based on polyacrylamide and chitosan and their

- interaction with ionic dyes,” *Carbohydr. Polym.*, vol. 88, no. 1, pp. 270–281, 2012, doi: 10.1016/j.carbpol.2011.12.002.
- [46] M. T. Taghizadeh, V. Siyahi, H. A.- Sorkhabi, and G. Zarrini, “ZnO , AgCl and AgCl / ZnO nanocomposites incorporated chitosan in the form of hydrogel beads for photocatalytic degradation of MB , E . coli and S . aureus,” *Int. J. Biol. Macromol.*, 2019, doi: 10.1016/j.ijbiomac.2019.10.070.
- [47] K. S. Anseth, C. N. Bowman, and L. Brannon-Peppas, “Mechanical properties of hydrogels and their experimental determination,” *Biomaterials*, vol. 17, no. 17, pp. 1647–1657, 1996, doi: 10.1016/0142-9612(96)87644-7.
- [48] R. Bellingeri *et al.*, “Nanocomposites based on pH-sensitive hydrogels and chitosan decorated carbon nanotubes with antibacterial properties,” *Mater. Sci. Eng. C*, 2018, doi: 10.1016/j.msec.2018.04.090.
- [49] B. K. D. O. BOZOĞLAN and TUNÇ Sibe, “Preparation and characterization of thermosensitive chitosan/carboxymethylcellulose/scleroglucan nanocomposite hydrogels,” *Mater. Des.*, vol. 186, p. 108334, 2020, doi: 10.1016/j.matdes.2019.108334.
- [50] K. Nesovic, A. Jankovi, A. Peri, Ž. Ljiljana, S. Park, and K. Y. Rhee, “Kinetic models of swelling and thermal stability of silver / poly ( vinyl alcohol )/ chitosan / graphene hydrogels,” vol. 77, pp. 83–96, 2019, doi: 10.1016/j.jiec.2019.04.022.
- [51] A. R. Karimi, M. Tarighatjoo, and G. Nikraves, “1,3,5-Triazine-2,4,6-tribenzaldehyde derivative as a new crosslinking agent for synthesis of pH-thermo dual responsive chitosan hydrogels and their nanocomposites : Swelling properties and drug release behavior,” *Int. J. Biol. Macromol.*, vol. 105, pp. 1088–1095, 2017, doi: 10.1016/j.ijbiomac.2017.07.128.
- [52] T. Caldas, R. Hernández, N. Rescignano, M. De Campos, and C. Mijangos, “Nanocomposite chitosan hydrogels based on PLGA nanoparticles as potential biomedical materials,” *Eur. Polym. J.*, 2017, doi: 10.1016/j.eurpolymj.2017.12.039.
- [53] N. Iglesias, E. Galbis, M. J. Díaz-Blanco, R. Lucas, E. Benito, and M. V. De-Paz, “Nanostructured Chitosan-based biomaterials for sustained and colon-specific resveratrol release,” *Int. J. Mol. Sci.*, vol. 20, no. 2, 2019, doi:

10.3390/ijms20020398.

- [54] S. Sauerbrunn and P. Gill, "Decomposition Kinetics Using TGA: High Resolution TGA Kinetics," no. TA075, [Online]. Available: [http://www.tainstruments.com/main.aspx?n=2&id=181&main\\_id=350&siteid=1](http://www.tainstruments.com/main.aspx?n=2&id=181&main_id=350&siteid=1)
- [55] P. Hong, S. Li, C. Ou, C. Li, L. Yang, and C. Zhang, "Thermogravimetric Analysis of Chitosan," 2007, doi: 10.1002/app.
- [56] H. Bai *et al.*, "Adsorption dynamics, diffusion and isotherm models of poly(NIPAm/LMSH) nanocomposite hydrogels for the removal of anionic dye Amaranth from an aqueous solution," *Appl. Clay Sci.*, vol. 124–125, pp. 157–166, 2016, doi: 10.1016/j.clay.2016.02.007.
- [57] M. Arango Muñoz, E. Arenas Castiblanco, and F. Cortés, "Determinación de parámetros cinéticos para la pirólisis rápida de aserrín de pino pátula," *Boletín del Grup. Español del Carbón*, no. 38, pp. 9–11, 2015.
- [58] E. S. Dragan, D. Felicia, and A. Loghin, "Fabrication and characterization of composite cryobeads based on chitosan and starches- g -PAN as efficient and reusable biosorbents for," *Int. J. Biol. Macromol.*, vol. 120, pp. 1872–1883, 2018, doi: 10.1016/j.ijbiomac.2018.10.007.
- [59] S. Li, B. Li, L. Gong, Z. Yu, Y. Feng, and D. Jia, "Enhanced mechanical properties of polyacrylamide / chitosan hydrogels by tuning the molecular structure of hyperbranched polysiloxane," *Mater. Des.*, vol. 162, pp. 162–170, 2019, doi: 10.1016/j.matdes.2018.11.045.
- [60] Y. Yang, X. Wang, F. Yang, H. Shen, and D. Wu, "A Universal Soaking Strategy to Convert Composite Hydrogels into Extremely Tough and Rapidly Recoverable," pp. 1–7, 2016, doi: 10.1002/adma.201601742.
- [61] C. Dannert, B. T. Stokke, and R. S. Dias, "Nanoparticle-hydrogel composites: From molecular interactions to macroscopic behavior," *Polymers (Basel)*, vol. 11, no. 2, 2019, doi: 10.3390/polym11020275.
- [62] Q. Xu, Y. Huang, M. Zeng, J. Chen, and Y. Wang, "Multi-structural network design and mechanical properties of graphene oxide filled chitosan-based

- hydrogel nanocomposites,” *Mater. Des.*, 2018, doi: 10.1016/j.matdes.2018.03.055.
- [63] B. Wu, D. Y. S. Yan, M. Khan, Z. Zhang, and I. M. C. Lo, “Application of magnetic hydrogel for anionic pollutants removal from wastewater with adsorbent regeneration and reuse,” *J. Hazardous, Toxic, Radioact. Waste*, vol. 21, no. 1, pp. 1–9, 2017, doi: 10.1061/(ASCE)HZ.2153-5515.0000325.
- [64] D. Jaspal and A. Malviya, “Composites for wastewater purification: A review,” *Chemosphere*, vol. 246, 2020, doi: 10.1016/j.chemosphere.2019.125788.
- [65] P. Domalik-pyzik and K. Pielichowska, “Chitosan-Based Hydrogels: Preparation, Properties, and Applications,” 2019.
- [66] V. Van Tran, D. Park, and Y. C. Lee, “Hydrogel applications for adsorption of contaminants in water and wastewater treatment,” *Environ. Sci. Pollut. Res.*, vol. 25, no. 25, pp. 24569–24599, 2018, doi: 10.1007/s11356-018-2605-y.
- [67] L. M. Sanchez, R. P. Ollier, J. S. Gonzalez, and V. A. Alvarez, *Nanocomposite materials for dyes removal*. Elsevier Inc., 2018.
- [68] Ñ. Crini and P. Badot, “Application of chitosan , a natural aminopolysaccharide , for dye removal from aqueous solutions by adsorption processes using batch studies : A review of recent literature,” vol. 33, pp. 399–447, 2008, doi: 10.1016/j.progpolymsci.2007.11.001.
- [69] K. Kaur and R. Jindal, “Comparative study on the behaviour of Chitosan-Gelatin based Hydrogel and nanocomposite ion exchanger synthesized under microwave conditions towards photocatalytic removal of cationic dyes,” *Carbohydr. Polym.*, vol. 207, no. November 2018, pp. 398–410, 2019, doi: 10.1016/j.carbpol.2018.12.002.
- [70] A. G. Ibrahim, A. Z. Sayed, H. Abd El-Wahab, and M. M. Sayah, “Synthesis of a hydrogel by grafting of acrylamide-co-sodium methacrylate onto chitosan for effective adsorption of Fuchsin basic dye,” *Int. J. Biol. Macromol.*, vol. 159, pp. 422–432, 2020, doi: <https://doi.org/10.1016/j.ijbiomac.2020.05.039>.
- [71] X. Liang *et al.*, “Ampholytic microspheres constructed from chitosan and carrageenan in alkali / urea aqueous solution for purification of various



- wastewater,” 2017, doi: 10.1016/j.cej.2017.02.089.
- [72] H. Y. Zhu, Y. Q. Fu, R. Jiang, J. Yao, L. Xiao, and G. M. Zeng, “Novel magnetic chitosan/poly(vinyl alcohol) hydrogel beads: Preparation, characterization and application for adsorption of dye from aqueous solution,” *Bioresour. Technol.*, vol. 105, pp. 24–30, 2012, doi: 10.1016/j.biortech.2011.11.057.
- [73] S. Li, “Removal of crystal violet from aqueous solution by sorption into semi-interpenetrated networks hydrogels constituted of poly ( acrylic acid-acrylamide-methacrylate ) and amylose,” *Bioresour. Technol.*, vol. 101, no. 7, pp. 2197–2202, 2010, doi: 10.1016/j.biortech.2009.11.044.
- [74] M. Akbarzadeh, M. T. Vardini, and G. R. Mahdavinia, “Preparation of a Novel Magnetic Nanocomposite Hydrogel Based on Carboxymethyl Chitosan for the Adsorption of Crystal Violet as Cationic Dye,” vol. 8, pp. 289–304, 2018, doi: 10.22034/jchr.2018.544709.
- [75] A. Vashist *et al.*, “Nanocomposite Hydrogels: Advances in Nanofillers Used for Nanomedicine,” *Gels*, vol. 4, no. 3, p. 75, 2018, doi: 10.3390/gels4030075.
- [76] A. K. Mishra, T. Masilompane, N. Chaukura, S. Mishra, and A. Mishra, “Chitosan-lignin-titania nanocomposites for the removal of brilliant black dye from aqueous solution,” *Int. J. Biol. Macromol.*, p. #pagerange#, 2018, doi: 10.1016/j.ijbiomac.2018.09.129.
- [77] A. Z. Moghaddam, E. Ghiamati, A. Pourashuri, and A. Allahresani, “Modified nickel ferrite nanocomposite / functionalized chitosan as a novel adsorbent for the removal of acidic dyes,” *Int. J. Biol. Macromol.*, vol. 120, pp. 1714–1725, 2018, doi: 10.1016/j.ijbiomac.2018.09.198.
- [78] M. E. A. Ali, “Synthesis and adsorption properties of chitosan- CDTA-GO nanocomposite for removal of hexavalent chromium from aqueous solutions,” *Arab. J. Chem.*, 2016, doi: 10.1016/j.arabjc.2016.09.010.
- [79] M. H. Beyki, F. Shemirani, and M. Shirkhodaie, “Aqueous Co(II) adsorption using 8-hydroxyquinoline anchored  $\gamma$  - Fe<sub>2</sub>O<sub>3</sub>@chitosan with Co(II) as imprinted ions,” *Int. J. Biol. Macromol.*, no. Ii, 2016, doi: 10.1016/j.ijbiomac.2016.02.077.

- [80] J. Wu, X. Cheng, Y. Li, and G. Yang, "Constructing biodegradable nanochitin-contained chitosan hydrogel beads for fast and efficient removal of Cu(II) from aqueous solution," *Carbohydr. Polym.*, vol. 211, no. January, pp. 152–160, 2019, doi: 10.1016/j.carbpol.2019.01.004.
- [81] G. Neeraj, S. Krishnan, P. S. Kumar, H. Cabana, and V. V. Kumar, "Adsorptive potential of dispersible chitosan coated iron-oxide nanocomposites towards the elimination of arsenic from aqueous solution," *Process Saf. Environ. Prot.*, 2016, doi: 10.1016/j.psep.2016.09.006.
- [82] S. Mallakpour and M. Madani, "Functionalized-MnO<sub>2</sub>/chitosan nanocomposites: A promising adsorbent for the removal of lead ions," *Carbohydr. Polym.*, vol. 147, pp. 53–59, 2016, doi: 10.1016/j.carbpol.2016.03.076.
- [83] E. Mirzaei B., A. Ramazani, M. Shafiee, and M. Danaei, "Studies on glutaraldehyde crosslinked chitosan hydrogel properties for drug delivery systems," *Int. J. Polym. Mater. Polym. Biomater.*, vol. 62, no. 11, pp. 605–611, 2013, doi: 10.1080/00914037.2013.769165.
- [84] T. Jóźwiak, U. Filipkowska, P. Szymczyk, J. Rodziewicz, and A. Mielcarek, "Effect of ionic and covalent crosslinking agents on properties of chitosan beads and sorption effectiveness of Reactive Black 5 dye," *React. Funct. Polym.*, vol. 114, pp. 58–74, 2017, doi: 10.1016/j.reactfunctpolym.2017.03.007.
- [85] S. R. G, P. Lakshmi, and E. Manjula, "Available online through phytopathogens," vol. 1, no. 6, pp. 114–117, 2010.
- [86] M. M. Beppu, R. S. Vieira, C. G. Aimoli, and C. C. Santana, "Crosslinking of chitosan membranes using glutaraldehyde: Effect on ion permeability and water absorption," *J. Memb. Sci.*, vol. 301, no. 1–2, pp. 126–130, 2007, doi: 10.1016/j.memsci.2007.06.015.
- [87] A. OU and I. BO, "Chitosan Hydrogels and their Glutaraldehyde-Crosslinked Counterparts as Potential Drug Release and Tissue Engineering Systems - Synthesis, Characterization, Swelling Kinetics and Mechanism," *J. Phys. Chem. Biophys.*, vol. 07, no. 03, 2017, doi: 10.4172/2161-0398.1000256.
- [88] E. Szymańska and K. Winnicka, "Stability of chitosan - A challenge for pharmaceutical and biomedical applications," *Mar. Drugs*, vol. 13, no. 4, pp.

1819–1846, 2015, doi: 10.3390/md13041819.

- [89] C. G. T. Neto, J. A. Giacometti, A. E. Job, F. C. Ferreira, J. L. C. Fonseca, and M. R. Pereira, “Thermal analysis of chitosan based networks,” *Carbohydr. Polym.*, vol. 62, no. 2, pp. 97–103, 2005, doi: 10.1016/j.carbpol.2005.02.022.
- [90] E. Goiti, M. M. Salinas, G. Arias, D. Puglia, J. M. Kenny, and C. Mijangos, “Effect of magnetic nanoparticles on the thermal properties of some hydrogels,” vol. 92, pp. 2198–2205, 2007, doi: 10.1016/j.polymdegradstab.2007.02.025.
- [91] J. Long *et al.*, “In situ synthesis of new magnetite chitosan/carrageenan nanocomposites by electrostatic interactions for protein delivery applications,” *Carbohydr. Polym.*, vol. 131, pp. 98–107, 2015, doi: 10.1016/j.carbpol.2015.05.058.
- [92] D. de Britto and S. P. Campana-Filho, “Kinetics of the thermal degradation of chitosan,” *Thermochim. Acta*, vol. 465, no. 1–2, pp. 73–82, 2007, doi: 10.1016/j.tca.2007.09.008.